CANCER

Fasting improves therapeutic response in hepatocellular carcinoma through p53-dependent metabolic synergism

Jelena Krstic[1], Isabel Reinisch[1], Katharina Schindlmaier[1], Markus Galhuber[1], Zina Riahi[1], Natascha Berger[1,2], Nadja Kupper[1], Elisabeth Moyschewitz[1], Martina Auer[1], Helene Michenthaler[1], Christoph Nössing[1,3], Maria R. Depaoli[4], Jeta Ramadani-Muja[4], Sinem Usluer[4], Sarah Stryeck[4,5,6], Martin Pichler[7], Beate Rinner[8], Alexander J. A. Deutsch[9], Andreas Reinisch[9,10], Tobias Madl[4,11], Riccardo Zenezini Chiozzi[12,13], Albert J. R. Heck[12,13], Meritxell Huch[14], Roland Malli[4,11], Andreas Prokesch[1,11]*

Copyright © 2022 The Authors, some rights reserved; exclusive licensee American Association for the Advancement of Science. No claim to original U.S. Government Works. Distributed under a Creative Commons Attribution NonCommercial License 4.0 (CC BY-NC).

Cancer cells voraciously consume nutrients to support their growth, exposing metabolic vulnerabilities that can be therapeutically exploited. Here, we show in hepatocellular carcinoma (HCC) cells, xenografts, and patient-derived organoids that fasting improves sorafenib efficacy and acts synergistically to sensitize sorafenib-resistant HCC. Mechanistically, sorafenib acts noncanonically as an inhibitor of mitochondrial respiration, causing resistant cells to depend on glycolysis for survival. Fasting, through reduction in glucose and impeded AKT/mTOR signaling, prevents this Warburg shift. Regulating glucose transporter and proapoptotic protein expression, p53 is necessary and sufficient for the sorafenib-sensitizing effect of fasting. p53 is also crucial for fasting-mediated improvement of sorafenib efficacy in an orthotopic HCC mouse model. Together, our data suggest fasting and sorafenib as rational combination therapy for HCC with intact p53 signaling. As HCC therapy is currently severely limited by resistance, these results should instigate clinical studies aimed at improving therapy response in advanced-stage HCC.

INTRODUCTION

Many cases of advanced-stage solid tumors show only temporary responses to targeted therapy because of the development of resistance against initially effective standard-of-care drugs. The ensuing residual disease (*1*) constitutes a severe impediment to progression-free patient survival. The adaptive nature (*2*) and metabolic flexibility of cancer cells (*3*) are key enabling mechanisms of resistance against targeted cancer therapy. Combination therapies represent promising strategies since they target several pathways, leaving less wiggle room for cancer cells to thrive on alternative growth-enhancing molecular routes.

Dietary interventions, particularly nutrient restriction regimens such as fasting or ketogenic diet, harbor a vast potential to support conventional cancer therapies (*4*, *5*). While nutrient restriction protocols vary considerably between studies (time-restricted feeding, every-other-day fasting, prolonged fasting for several days, or diets restricted in certain nutrients or in calories) (*5*), common denominators are systemic changes in metabolites (mainly glucose, ketone bodies, and amino acids), hormones (e.g., insulin, glucagon, and glucocorticoids), and growth factors (most prominently insulin-like growth factor 1) (*6*). The rationale underlying the use of fasting in cancer therapy is based on specific and general features of cancer cells: They disobey antigrowth signals (*7*) and have a pronounced anabolic appetite (*8*, *9*). Therefore, cancer cells are unable to properly adapt to fasting conditions (*10*). A large number of preclinical studies support this reasoning by showing reduced tumorigenesis, alleviation of therapy resistance, or reduced adverse effects when different fasting regimens are combined with standard-of-care drugs (*10*–*12*). Several clinical trials are ongoing [reviewed in (*13*)] and will soon deliver data about the applicability and translatability of data from animal models. Note, however, that the responses to fasting are specific to cancer types and their mutational landscapes (*5*). Hence, focused studies need to validate fasting/drug combinations, factoring in cancer type and patient and intratumor heterogeneity, to enable stratification approaches as recently suggested (*4*).

Hepatocellular carcinoma (HCC) is the primary form of liver cancer (*14*) and is one of the deadliest cancers worldwide with rising incidence (*15*). This is due to the lack of response to classical chemotherapeutics (e.g., doxorubicin and cisplatin) and targeted drugs in early-stage disease (*16*). For late-stage HCC, sorafenib has long been the mainstay in first-line treatment (*17*) and is still frequently used where other more expensive drugs are not available or upon progression after atezolizumab/bevacizumab in later treatment lines (*18*, *19*). Sorafenib has been shown to act as a multiple-kinase inhibitor on the endothelial cell compartment (antiangiogenic via, e.g., vascular

[1]Gottfried Schatz Research Center for Cell Signaling, Metabolism and Aging, Division of Cell Biology, Histology and Embryology, Medical University of Graz, 8010 Graz, Austria. [2]Department of Obstetrics and Gynecology, Medical University of Graz, 8036 Graz, Austria. [3]Cancer Research UK Beatson Institute, Garscube Estate, Glasgow, UK. [4]Gottfried Schatz Research Center for Cell Signaling, Metabolism and Aging, Division of Molecular Biology and Biochemistry, Medical University of Graz, 8010 Graz, Austria. [5]Institute of Interactive Systems and Data Science, Graz University of Technology, 8010 Graz, Austria. [6]Know-Center GmbH, 8010 Graz, Austria. [7]Division of Clinical Oncology, Department of Medicine, Comprehensive Cancer Center Graz, Medical University of Graz, 8036 Graz, Austria. [8]Department for Biomedical Research, Medical University of Graz, Graz, Austria. [9]Division of Hematology, Department of Internal Medicine, Medical University of Graz, 8036 Graz, Austria. [10]Division of Hematology, Department of Blood Group Serology and Transfusion Medicine Medical University of Graz, 8036 Graz, Austria. [11]BioTechMed-Graz, 8010 Graz, Austria. [12]Biomolecular Mass Spectrometry and Proteomics, Bijvoet Center for Biomolecular Research and Utrecht Institute of Pharmaceutical Sciences, Utrecht University, 3584CH Utrecht, Netherlands. [13]Netherlands Proteomics Center, 3584CH Utrecht, Netherlands. [14]Max Planck Institute of Molecular Cell Biology and Genetics, 01307 Dresden, Germany.
*Corresponding author. Email: andreas.prokesch@medunigraz.at

Downloaded from https://www.science.org on February 16, 2022

endothelial growth factor inhibition) and on hepatocytes [mainly as rapidly accelerated fibrosarcoma (RAF) inhibitor] (*20*). In a landmark placebo-controlled clinical trial, sorafenib was shown to improve overall survival by 3 months with no case of complete remission (*21*). This modest therapy success is largely ascribed to the development of sorafenib resistance (*20*). While several mechanisms of resistance have been suggested, many reports converge on hyperactivation of phosphatidylinositol 3-kinase (PI3K)/AKT/mTOR and mitogen-activated protein kinase (MAPK) signaling upon sorafenib treatment [reviewed in (*20*)]. Thus, there is a need for novel treatment approaches and combination therapies that improve the current clinical situation for patients with HCC.

Here, we show in vivo and in vitro evidence that nutrient restriction can sensitize sorafenib-resistant HCC models and improve the efficacy in sorafenib-responsive models. We pinpoint the mechanism of sensitization to a synergistic action of sorafenib, as a potent inhibitor of mitochondrial respiration, and starvation or fasting, which prevents a Warburg shift by limiting glucose availability. We further show that p53 is necessary for this sensitization by coordinating glucose uptake and proapoptotic protein expression. Together, our data suggest fasting as a potent adjuvant to sorafenib in p53-positive HCC and should inspire clinical studies that scrutinize this rational polytherapy approach.

RESULTS

Nutrient restriction synergistically sensitizes resistant HCC cells, xenografts, and patient-derived HCC organoids to sorafenib

Intrinsic and acquired sorafenib resistance is a major impediment to progression-free survival in late-stage HCC (*20*), and novel combination therapies to overcome resistance are needed. To investigate whether starvation can alleviate sorafenib resistance, we tested the responsiveness of HCC-derived HepG2 cells to sorafenib. Confirming previous studies (*22*), HepG2 cells stayed largely resistant to sorafenib up to supraclinical doses (fig. S1A). In patients with HCC, plasma sorafenib levels range between 5 and 20 μM after oral application (*23*, *24*). Next, we subcutaneously injected these cells in NMRI nude mice and randomly divided them into four groups receiving either vehicle control or sorafenib and further in groups that were kept on ad libitum diet, on a periodic fasting regimen (fasted), or on a fasting-mimicking diet (FMD) (Fig. 1A) (*25*). For the fasted group, mice were withheld food for 24 hours two times a week, with 2 or 3 days of ad libitum refeeding in between. While this protocol robustly elicited fasting-mediated changes in plasma metabolites (fig. S1B), mice were able to fully regain the weight loss during the refeeding days (Fig. 1B). Less gentle fasting protocols such as every-other-day fasting led to progressive weight loss (fig. S1, D and F), rendering this regimen unsuitable for prolonged treatment protocols. Sorafenib or vehicle control was orally applied at the beginning of the refeeding phase at a concentration of 30 mg/kg (toxicity was evaluated in separate experiments; fig. S1, G to I) (*21*). Tumor growth was affected neither by sorafenib treatment nor by fasting alone (Fig. 1, C and D). However, combined treatment over 4 weeks significantly stunted in vivo tumor growth (Fig. 1, C and D). Histological analyses showed no difference in the staining of the proliferation marker Ki67 (fig. S1J), while a trend to larger patches of necrotic cells was observed in the combination treatment group as compared to sorafenib alone (fig. S1K). Similar to the periodic fasting, xenograft experiments with FMD and sorafenib (60 mg/kg) (Fig. 1A) did also conserve body weight over the treatment period (Fig. 1E). The combination of FMD and sorafenib (60 mg/kg) showed a significant additive effect (Fig. 1, F and G), while the single treatments only showed a trend to reduction in final tumor size (Fig. 1G). These results indicate that periodic fasting or FMD can alleviate sorafenib resistance in a synergistic or additive manner, respectively.

To mechanistically investigate this synergism, we sought to mimic the nutrient restriction in vitro. For this, we used Hanks' balanced salt solution (HBSS)–based starvation medium (SM) shown to induce autophagy in cultured liver cells (*26*) and to activate the fasting-responsive AMPK pathway in HepG2 cells (*27*). When resistant HepG2 cells (fig. S1A) were kept in SM for 24 hours, we observed a sorafenib dose-dependent reduction in viability, while starvation alone did not reduce viability (Fig. 1, H and I). These effects were exaggerated when viability was determined after 48 hours of treatment (fig. S1, L and M). Furthermore, cytotoxicity (Fig. 1J) and apoptosis (Fig. 1K and fig. S1N) were increased in a sorafenib dose-responsive manner in starved cells but not in cells kept in full growth medium (GM). To gain insight into the kinetics of the synergistic effect, we continuously monitored the cells using a real-time apoptosis/necrosis assay. As shown in the right of Fig. 1L, the apoptotic signal was already elevated 4 hours after the beginning of the combination treatment, while necrosis did not occur within the observed time frame.

To confirm these results in patient-derived material, we used HCC organoids described previously to be sorafenib-resistant (*28*). Maintaining these tumoroids in a starvation-mimicking medium did not per se impede their viability (Fig. 1, M and N). However, compared to full expansion medium (*29*), starvation-mimicking medium elicited a dose-dependent decrease in viability in response to sorafenib (Fig. 1N), resembling results in HepG2 cells (e.g., Fig. 1I).

Opposing the sensitization of transformed and resistant HCC models, the viability of mouse primary hepatocytes was largely unaffected by sorafenib with or without starvation in different exposure protocols (fig. S1, O and P). This suggests that sorafenib selectively targets HCC cells, while leaving nontransformed hepatocytes unharmed, which is mirrored by our pilot experiments (fig. S1, G to I). Furthermore, our data are in line with a recent study showing beneficial effects on liver pathology of sorafenib at doses similar to the ones used in our study (*30*). Together, these results show that nutrient restriction synergizes with sorafenib to alleviate therapy resistance by activating cell death programs in cultivated cells, HCC organoids, and xenografts.

Sorafenib/starvation synergism is specific but does not act via canonical kinase inhibition or single starvation-responsive pathways

To test whether the synergism between starvation and sorafenib is a specific phenomenon, we next investigated cotreatment with starvation and doxorubicin, a chemotherapeutic that was recently used in an HCC trial in combination with sorafenib (*31*). Effective doses of doxorubicin (shown by p53 stabilization in response to doxorubicin-induced DNA damage in fig. S2A) led to a marginal decrease in cell viability under starvation conditions (Fig. 2A). Consistent with previous clinical studies that showed no beneficial effects of doxorubicin over sorafenib treatment or after the failure of sorafenib treatment (*32*), we did not observe any additional effect over sorafenib/doxorubicin combination treatment, regardless of the cells being

Downloaded from https://www.science.org on February 16, 2022

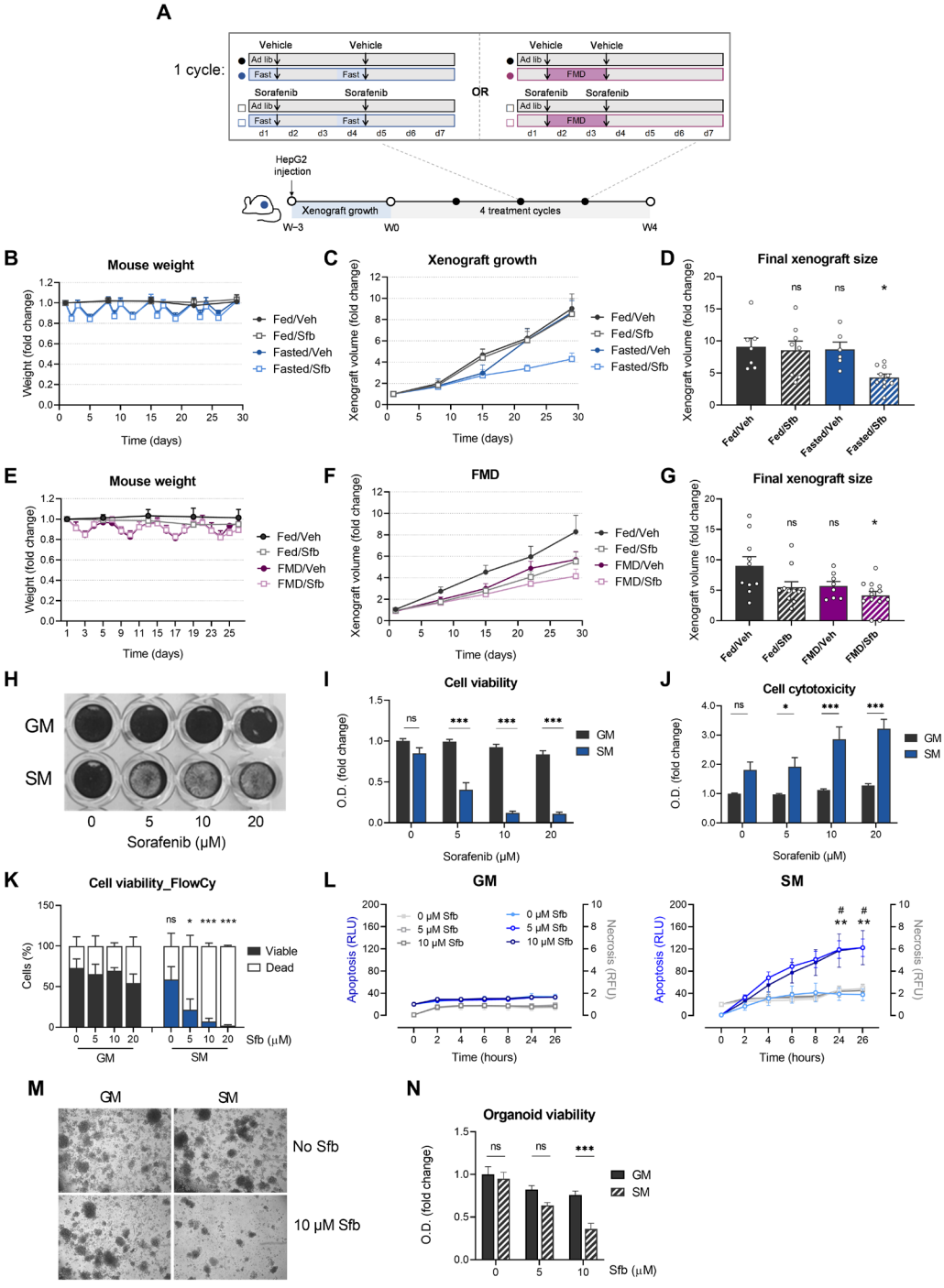

Fig. 1. Nutrient restriction synergistically sensitizes resistant HCC cells, xenografts, and patient-derived HCC organoids to sorafenib. (**A**) Experimental design (described in Materials and Methods). (**B** and **E**) Animal weight, normalized to starting the weight of each group. Mean values ± SD are shown; $n = 6$ to 10 per group. (**C** and **F**) Xenograft volume normalized to the initial volume. (**D** and **G**) Final xenograft volumes (at day 29). All groups compared to fed/Veh group; one-way ANOVA and Dunnett's multiple comparisons test. (**H**) HepG2 cells stained with Gentian violet after 24 hours of incubation in growth medium (GM) or starvation medium (SM) with indicated sorafenib (Sfb) concentrations. (**I**) Viability of HepG2 cells after 24 hours of incubation in GM or SM with indicated Sfb concentrations. Normalized to nontreated cells grown in GM. (**J**) Cytotoxicity in cells grown in GM versus SM with indicated Sfb concentrations after 24 hours. (**K**) Percentage of viable (7-AAD and annexin V negative) and dead (7-AAD and/or annexin V positive) cells analyzed by flow cytometry. SM groups compared to corresponding GM groups. (**L**) Apoptosis (blue lines) and necrosis (gray lines) of HepG2 cells measured during 24 hours in GM (left) and SM (right). Two-way ANOVA and Dunnett's multiple comparisons test. Each group compared to control (GM/0). *SM/5 μM Sfb versus GM/0; #SM/10 μM Sfb versus GM/0. (**M** and **N**) HCC patient-derived organoids were incubated for 6 days in GM or SM (as described in Materials and Methods) with or without Sfb. (M) Microscope images showing a decreased number of organoids in combination treatment. (N) Organoid viability. If not noted otherwise, mean values ± SEM are shown, and two-way ANOVA and Tukey's multiple comparisons test were performed. ***$P < 0.001$, **$P < 0.01$, and *$P < 0.05$; ns, not significant ($P > 0.05$); O.D., optical density; RLU, relative luminescence units; RFU, relative fluorescence units.

Downloaded from https://www.science.org on February 16, 2022

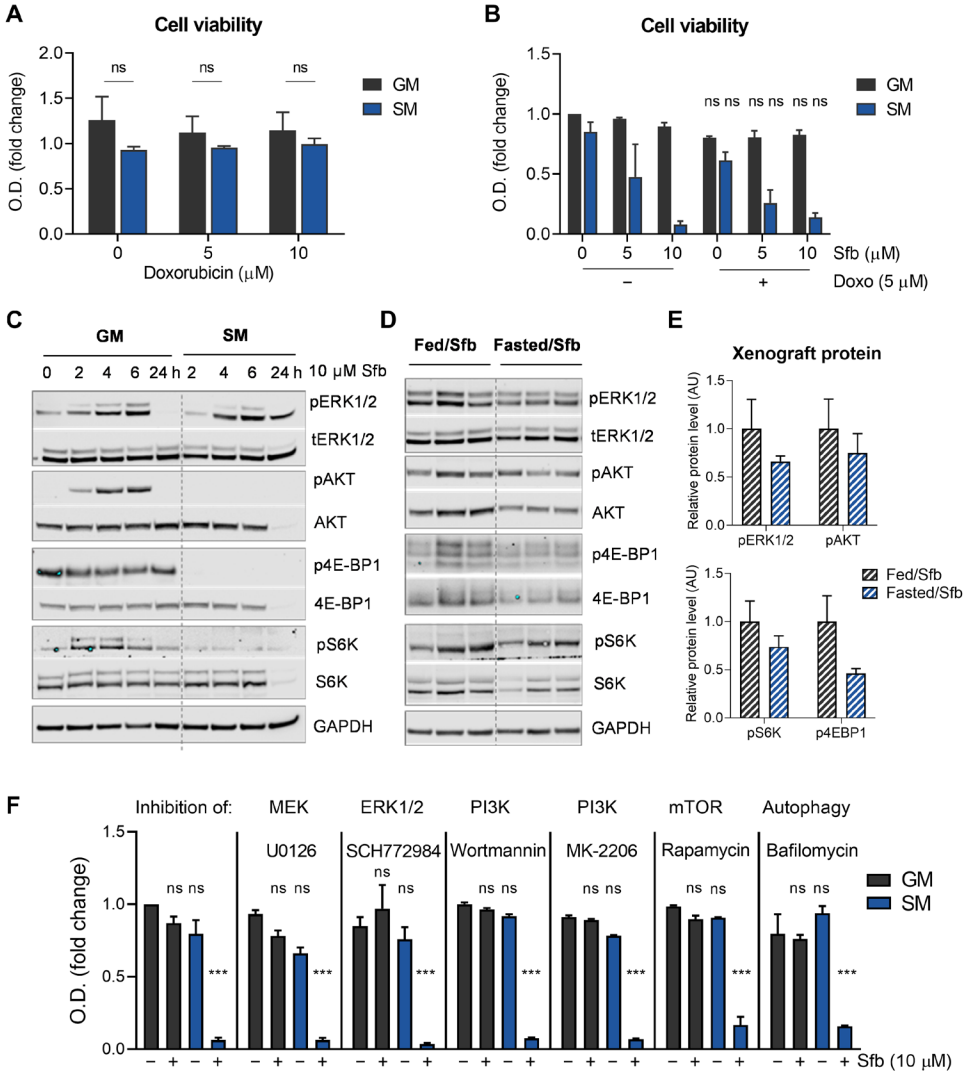

Fig. 2. Sorafenib/starvation synergism is specific but does not act via canonical kinase inhibition or single starvation-responsive pathways. (**A**) Viability of HepG2 cells after 24 hours of incubation in GM or SM with indicated concentrations of doxorubicin (Doxo). Values are normalized to the viability of nontreated cells grown in GM. (**B**) Viability of HepG2 cells after 24 hours of incubation in GM or SM with indicated concentrations of Doxo and/or sorafenib (Sfb). Values are normalized to the viability of nontreated cells grown in GM. Comparison of groups treated with Doxo and Sfb versus corresponding groups treated with Sfb is shown. (**C**) HepG2 cells were grown in GM or SM with 10 μM Sfb for the indicated times, and Western blot analysis was performed to determine protein levels of AKT, ERK, 4E-BP1, and S6K and their respective phosphorylated forms. Glyceraldehyde-3-phosphate dehydrogenase (GAPDH) served as a loading control. (**D**) Western blot analysis was performed to determine protein levels of AKT, ERK, 4E-BP1, and S6K and their respective phosphorylated forms in HepG2 xenografts from ad libitum fed and fasted nude mice treated with Sfb (30 mg/kg). GAPDH served as a loading control. (**E**) Quantification of phosphorylated protein levels, relative to GAPDH and normalized to the protein level in xenograft protein lysates from fed mice. Unpaired *t* test was performed. AU, arbitrary units. (**F**) Viability of HepG2 cells after 24 hours of incubation in GM or SM with Sfb and/or MEK inhibitor (5 μM U0126), ERK1/2 inhibitor (1 μM SCH772984), PI3K inhibitor (1 μM wortmannin), PI3K inhibitor (1 μM MK-2206), 10 nM rapamycin, and 10 nM bafilomycin was determined. Comparison of groups within each inhibitor treatment group is shown. If not noted otherwise, mean values ± SEM are shown, and two-way ANOVA and Tukey's multiple comparisons test were performed. ***$P < 0.001$; ns, not significant ($P > 0.05$); AU, arbitrary units.

maintained in full GM or SM (Fig. 2B). Hence, these data suggest that drug sensitization is achieved when starvation is combined with sorafenib but not when combined with the chemotherapeutic doxorubicin.

In transformed hepatocytes, sorafenib was initially identified targeting RAF kinases to inhibit the RAS-RAF-MEK-ERK pathway (*33*). Instead of inhibiting this pathway, sorafenib led to increased phosphorylation of extracellular signal–regulated kinase (ERK) (Fig. 2C) in resistant HepG2 cells, reminiscent of previous reports describing a paradoxical activation of this pathway by sorafenib and other BRAF inhibitors (*34*, *35*). To test whether sorafenib acts via inhibition of other growth pathways, we investigated the fasting-responsive PI3K-AKT-mTOR pathway (*10*, *36*), hyperactivation of which is a common denominator of malignant reprogramming in many cancers (*37*). Probing activation of AKT through phosphorylation of serine-473, we found that sorafenib treatment leads to a dynamic activation of AKT (Fig. 2C). This could represent a compensatory response to boost glycolysis as reported in other cancer models (*9*)

Downloaded from https://www.science.org on February 16, 2022

and a potential mechanism of resistance to sorafenib in our system. However, in SM that only contains low glucose (5.5 mM, as opposed to 25 mM in full GM) and no growth factors, AKT activity is completely abrogated (Fig. 2C), coinciding with sensitivity to sorafenib. mTORC1 was also activated under sorafenib treatment in normal GM but was completely blunted through starvation as evidenced by a loss of phosphorylation of mTORC1 substrates S6K1 and 4EBP-1 (Fig. 2C). This reduction of growth pathways by combination treatment was largely recapitulated by analyzing tumors from the xenograft assay (Fig. 2, D and E).

Targeted pharmacological inhibition (fig. S2, B to F) of MAPK kinase (MEK), ERK, PI3K, AKT, and mTORC1, as well as of autophagy (downstream of mTORC1) (*37*), did neither recapitulate sorafenib effects under starvation nor show any additional effects over starvation/sorafenib cotreatment on cell viability (Fig. 2F). This set of experiments rules out these pathways as the sole mediators of starvation-mediated sensitization to sorafenib.

Thus, the paradoxical up-regulation of several growth pathways in response to sorafenib treatment could constitute a resistance mechanism in our model (*20*). Overcoming this resistance seems not to rely on single growth pathways but rather on the pleiotropic effects of starvation affecting the PI3K-AKT-mTORC1 axis that, in combination with noncanonical sorafenib action, leads to HCC cell death.

Sorafenib-induced Warburg shift is curtailed by glucose limitation under starvation

Several previous studies have described the impact of sorafenib on mitochondrial bioenergetics (*30*, *38*, *39*). Furthermore, AKT activation boosts aerobic glycolysis in cancer cells with defective mitochondria (*40*). We therefore investigated whether such a Warburg shift, a hallmark of cellular transformation (*9*), could be the underlying mechanism of resistance in our model.

We first evaluated oxygen consumption rate (OCR), reflecting mitochondrial oxidative phosphorylation (OXPHOS), in sorafenib-resistant HepG2 cells after 6 hours of treatment, when cell viability was uncompromised under all conditions (fig. S3A) and AKT is maximally activated (Fig. 2C). As shown in Fig. 3 (A and B), starvation led to a dampening, and sorafenib treatment to a severe reduction, of the basal and stimulated OCR. Showing a potent additive effect, combination treatment completely obliterated any cellular respiration within 6 hours after treatment. Basal OCR, adenosine triphosphate (ATP)–linked OCR, and maximal respiration were significantly reduced by either treatment alone and largely undetectable after the combination treatment (Fig. 3B). Refeeding cells for 2 hours after pretreatment with sorafenib, starvation, or both showed that the starvation-mediated OCR attenuation is completely reversible, while sorafenib treatment caused a prolonged inhibition of cellular respiration (Fig. 3C), indicative of persistent inhibition of OXPHOS. Next, we determined the mitochondrial membrane potential. Starvation alone did not affect mitochondrial membrane potential (fig. S3B). However, 2 and 6 hours of sorafenib treatment significantly reduced mitochondrial membrane potential (Fig. 3D) while leaving mitochondrial morphology intact (Fig. 3E). Because the effect of sorafenib on mitochondrial ATP-linked OXPHOS was most pronounced in GM (Fig. 3, A and B), we reasoned that the cells might execute a Warburg shift toward aerobic glycolysis to enable survival. Thus, we monitored glycolytic function in real time upon acute treatment with sorafenib or oligomycin, an ATP synthase inhibitor. Sorafenib was as potent as oligomycin in stimulating the extracellular acidification rate (ECAR), a proxy for glycolytic activity (Fig. 3F). A 6-hour sorafenib treatment in full GM led to increased levels of ECAR from nonglucose substrates (measurements before glucose injection) and after glucose and oligomycin addition, consistent with a Warburg shift (Fig. 3G, left). However, cells pretreated in SM showed no metabolic flexibility upon sorafenib treatment (Fig. 3G, right), although acute addition of glucose can reinstate glycolysis to the maximal glycolytic capacity (Fig. 3G, right). These data led us to hypothesize that, while sorafenib induces persistent OXPHOS inhibition eliciting a Warburg shift to glycolysis, starvation can acutely curtail this shift and thereby reduce cancer cell survival. This would imply that starvation uses a metabolic window of opportunity opened by sorafenib action as an OXPHOS inhibitor in our system. Notably, the SM contains low levels of glucose (5.5 mM) compared to standard GM (25 mM). Therefore, after 6 hours of treatment, this glucose level might still be sufficient for starved and sorafenib-treated cells to remain viable (fig. S3A) by increasing their glycolysis rate (shown by increased ECAR in Fig. 3B).

To identify the major metabolite responsible for the sensitization effect of starvation, we used Dulbecco's modified Eagle's medium (DMEM) without glucose, pyruvate, glutamine, and fetal calf serum (FCS) ($DMEM^{-/-/-}$) and observed the viability upon individual add-back of these components. Corroborating data from above, showing that the addition of glucose immediately rescues glycolytic function (Fig. 3G), only glucose add-back maintained cell viability, while add-back of neither glutamine nor pyruvate rescued viability (Fig. 3H). FCS, rich in growth factors, hormones, and metabolites, had a marginal effect in increasing viability upon addition to $DMEM^{-/-/-}$ (Fig. 3H). This experiment indicated that glucose may be the primary metabolite responsible for the sorafenib sensitization effect of starvation. Confirming this, a titration add-back experiment showed that cell viability upon sorafenib treatment was gradually rescued with increasing glucose doses (Fig. 3I). To compare these in vitro glucose concentrations to the in vivo situation, we measured plasma glucose (Fig. 3J) and tumor interstitial fluid glucose levels (Fig. 3K) in fed and fasted mice in the xenograft experiment. Both plasma and interstitial fluid glucose levels were significantly reduced to ~3 mM by fasting, a concentration that does not inflict a rescue of cell viability in the in vitro titration (Fig. 3I). On the other hand, with 5 mM glucose add-back (levels comparable to plasma and interstitial fluid fed glucose levels), ~50% of cells were viable, indicating that our in vitro experiments reflect the glucose levels, and with that the effects, in the tumor microenvironment and vice versa. To assess the impact of glucose on survival under sorafenib treatment directly, we treated cells kept in full GM with sorafenib and increasing concentrations of the glycolysis inhibitor 2-deoxy-D-glucose (2-DG). Starting with a stoichiometric ratio of 1:4 (glucose:2-DG), cell viability was significantly decreased after 24 hours (Fig. 3L), robustly establishing glucose as the limiting metabolite required for sorafenib sensitization through starvation. This was confirmed for sorafenib-resistant HCC organoids (Fig. 1, M and N), as inhibition of glycolysis by 2-DG in full medium significantly reduced their viability (Fig. 3M).

Together, our data indicate that sorafenib acts noncanonically as an OXPHOS inhibitor initiating a Warburg shift to aerobic glycolysis in HepG2 cells. Starvation or fasting curtails this metabolic flexibility through the limitation of glucose and, with that, confers sensitivity toward the anticancer effects of sorafenib.

Downloaded from https://www.science.org on February 16, 2022

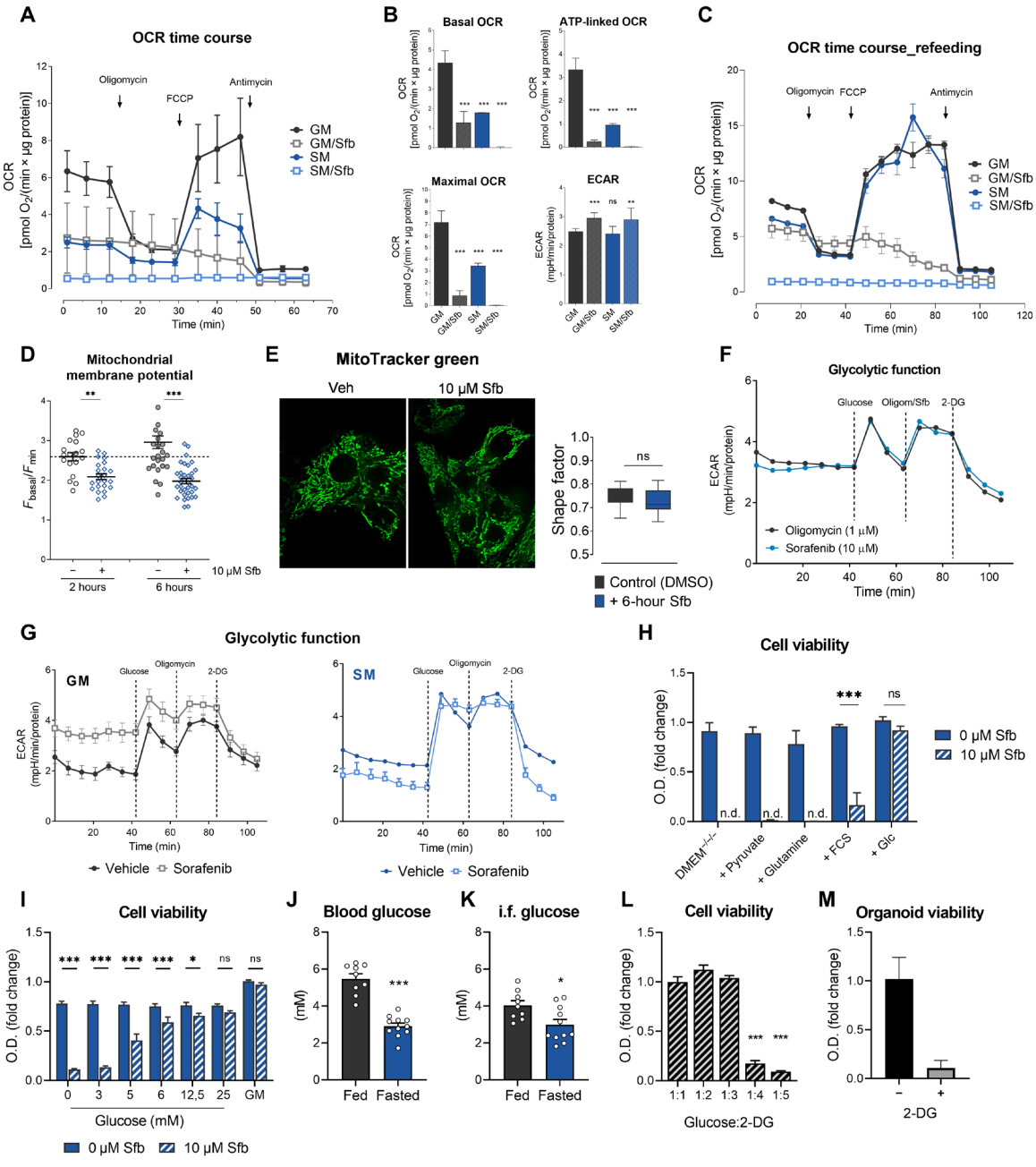

Fig. 3. Sorafenib-induced Warburg shift is curtailed by glucose limitation under starvation. (**A**) Continuous OCRs in HepG2 cells after 6 hours of incubation in GM or SM with 0 or 10 µM sorafenib (Sfb). (**B**) Basal respiration, ATP-linked respiration, maximal respiration, and ECAR compared to GM group. (**C**) Continuous OCR in HepG2 cells after 2 hours of refeeding with GM. (**D**) Mitochondrial membrane potential in HepG2 cells after incubation with vehicle (DMSO) or 10 µM Sfb. (**E**) MitoTracker green mitochondrial staining in HepG2 cells (left) after 6 hours of treatment with 10 µM Sfb and signal quantification (right). (**F**) Glycolysis stress test in HepG2 cells grown in GM. (**G**) Glycolysis stress test in HepG2 cells grown in GM (left) or SM (right) with or without 10 µM Sfb for 6 hours. (**H**) HepG2 cell viability after 24 hours of incubation in DMEM without glucose, glutamine, and pyruvate (DMEM$^{-/-/-}$) or with added media components, with or without 10 µM Sfb. n.d., not detected. (**I**) HepG2 cell viability after 24 hours of incubation in DMEM$^{-/-/-}$ or with indicated glucose concentrations. (**J**) Blood glucose concentration in xenografted NMRI nude mice after 24 hours of fasting. (**K**) Glucose concentration in the interstitial fluid (i.f.) of xenografts from fed and 24-hour fasted mice. (**L**) HepG2 cell viability after 24 hours of incubation in GM with 10 µM Sfb and 2-deoxy-D-glucose (2-DG) in indicated molar ratios to glucose. One-way ANOVA and Tukey's multiple comparisons test, compared to 1:1 group. (**M**) Organoid viability after 6 days of incubation in GM with 5 µM Sfb and with or without 50 mM 2-DG (1:2 ratio to glucose). Mean values ± SEM are shown. (B, H, and I) Two-way ANOVA and Tukey's multiple comparisons test. (D, E, J, K, and M) Unpaired *t* test. ***$P < 0.001$, **$P < 0.01$, and *$P < 0.05$; ns, not significant ($P > 0.05$); n.d., not detected.

Downloaded from https://www.science.org on February 16, 2022

p53 is required for the synergistic antitumorigenic action of starvation and sorafenib

Loss of function of the tumor suppressor and transcription factor p53 is causative for or involved in the development of more than 50% of human cancers (*41*), and ~30% of HCC cases present with a mutation in the gene coding for p53. Apart from its tumor suppressor function, p53 is increasingly appreciated as a regulator of cancer metabolism (*42*), and we recently published that the *TP53* protein is stabilized in starved HepG2 cells, leading to activation of downstream target genes (*27*).

To investigate the influence of p53 on starvation-mediated sensitization to sorafenib, we used CRISPR-Cas9 to derive *TP53* knockout (p53KO) clones from resistant HepG2 cells (fig. S4, A and B). Isogenic p53KO cells treated with the same starvation/sorafenib protocol used for their p53-proficient counterparts (Fig. 1I) did not show a significant decrease in viability (Fig. 4A) or an increase of cytotoxicity (Fig. 4B), which renders p53-deficient cells resistant to sorafenib even under starvation conditions. To exclude potential clonal effects, we validated this observation in other CRISPR-Cas9 clones (fig. S4C) and reexpressed *TP53* in the p53KO cells (fig. S4D). The reexpression of p53 reinstated target gene expression (fig. S4E) and sensitization to sorafenib under starvation (Fig. 4C, right), indicating that p53 is necessary and sufficient for this synergistic effect.

We next xenografted p53KO cells in nude mice and subsequently subjected them to the same periodic fasting/sorafenib protocol (illustrated in Fig. 4D and fig. S4F) as for p53-proficient HepG2 cells [p53 wild type (p53WT)] (Fig. 1A). Immunohistochemistry (Fig. 4E), Western blot (Fig. 4F), and quantitative polymerase chain reaction

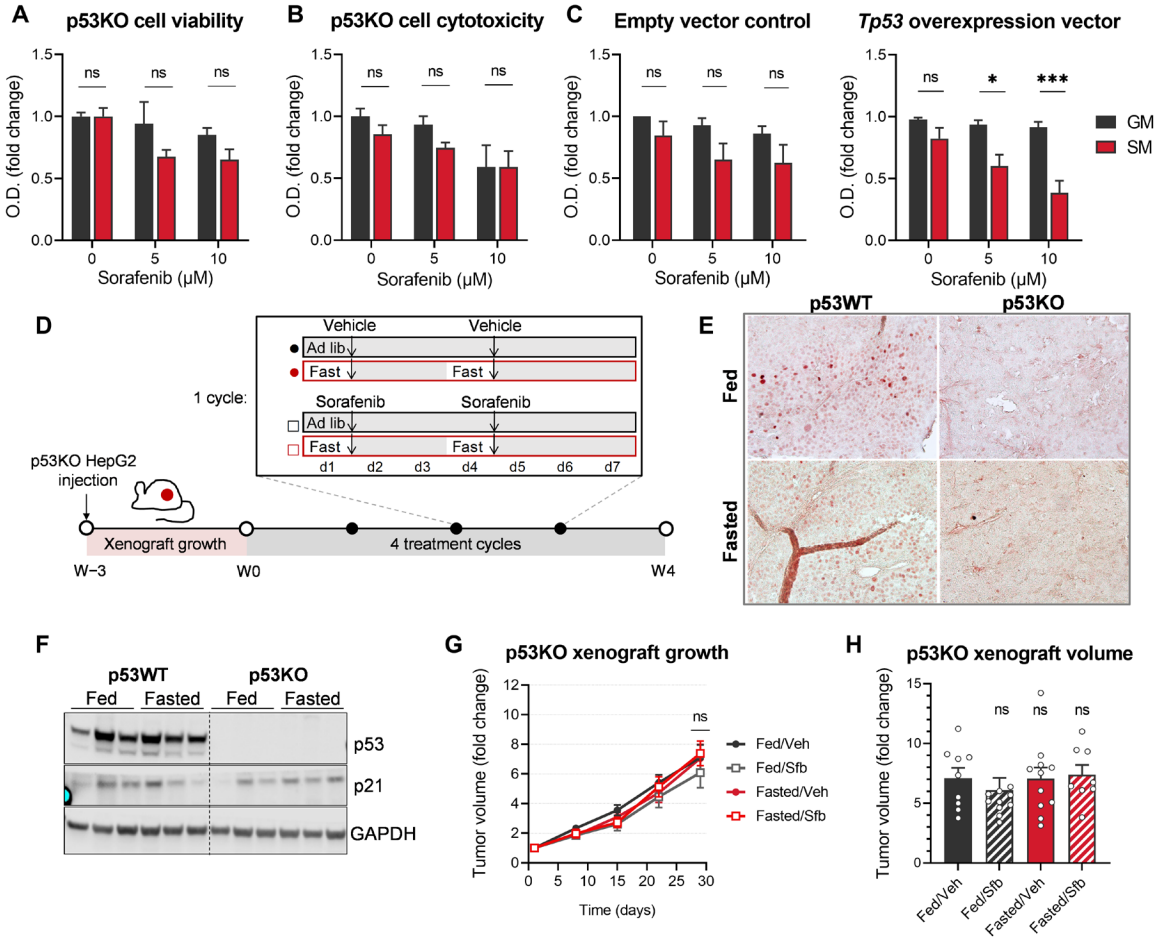

Fig. 4. p53 is required for the synergistic antitumorigenic action of starvation and sorafenib. (**A**) Viability of HepG2 p53KO cells after 24 hours of incubation in GM or SM with indicated concentrations of Sfb. Values are normalized to the viability of nontreated cells grown in GM. (**B**) Cytotoxicity measured by LDH assay in p53KO cells grown in GM versus cells grown in SM with indicated Sfb concentrations after 24 hours. (**C**) p53KO cells were transfected with an empty vector (left) and p53 overexpression vector (right). Viability assay was performed after 24 hours of incubation in GM or SM with indicated concentrations of Sfb. (**D**) Experimental design: After p53KO HepG2 cells that were injected into the hind flanks of NMRI Foxn1$^{nu/nu}$ mice formed palpable xenografts, mice were divided into four groups as described in Fig. 1A. (**E**) Immunohistochemical staining of p53 in xenograft sections from mice injected with p53WT and p53KO HepG2 cells. (**F**) Western blot analysis was performed to determine protein levels of p53 and p21 in xenografts from ad libitum fed and fasted nude mice. GAPDH served as a loading control. (**G**) Xenograft volume normalized to its starting volume; $n = 8$ to 11 per group. Two-way ANOVA and Dunnett's multiple comparisons test, all groups compared to fed/Veh group. (**H**) Relative xenograft volumes at day 29. One-way ANOVA and Tukey's multiple comparisons test, comparison of each group versus control, and fed/Veh group is shown; $n = 8$ to 11 per group. If not noted otherwise, mean values ± SEM are shown, and two-way ANOVA and Tukey's multiple comparisons test were performed. ***$P < 0.001$ and *$P < 0.05$; n.s., not significant ($P > 0.05$).

Downloaded from https://www.science.org on February 16, 2022

(qPCR; fig. S4G) assessing p53 and p53 target gene expression confirmed persistent KO throughout the in vivo tumor growth assay. Subcutaneous tumor growth rates were similar in all four groups (Fig. 4, G and H), confirming in vivo that p53 is required for the synergistic effect of fasting/starvation and sorafenib.

p53 confers starvation/sorafenib synergism by regulating glycolytic rate and capacity

To decipher the mechanistic aspects of p53 status on the synergism of sorafenib and starvation, we first investigated growth pathways and cancer cell metabolism. p53WT (Fig. 2C) and p53KO cells showed similar activation of ERK, AKT, and mTORC1 pathways when treated with sorafenib in GM and a similar abrogation of AKT and mTORC1 signaling in SM (Fig. 5A). Combination treatment completely blocked OXPHOS in p53KO just as in p53WT cells (fig. S5A), while the glycolytic rate and capacity in p53KO cells were lower (Fig. 5, B and C) when compared to p53WT cells. p53WT cells retain their glucose uptake at a similar level in both control and combination treatment, while p53KO cells significantly reduce glucose uptake upon combination treatment (Fig. 5, D and E). Corresponding with reduced glucose uptake, the most abundant glucose transporter in liver cells (*SLC2A2*) was strongly down-regulated in p53-deficient cells (Fig. 5F). Furthermore, glucose transporter down-regulation (*SLC2A1*, *SLC2A2*, and *SLC2A3*) was also observed in p53KO xenografts after 4 weeks of combined treatment (Fig. 5G). Complete depletion of glucose severely dampened p53KO cells' survival under sorafenib treatment, and only add-back of glucose, but not pyruvate, glutamine, or FCS (fig. S5B), was sufficient to reinstate sorafenib resistance in p53KO cells (Fig. 5H and fig. S5B). Accordingly, blockage of glycolysis with 2-DG and concomitant sorafenib treatment led to p53KO cell death (Fig. 5I). These results demonstrate that p53KO cells under combination treatment reduce the expression of glucose transporters, resulting in reduced glucose uptake and lower glycolytic rate and capacity compared to p53WT cells. While p53KO cells are as dependent on glucose as p53WT cells, their "economic" use of the little glucose in the SM could prolong their survival.

p53 coordinates the proapoptotic proteome during combination treatment

To further dissect why p53 is necessary for the synergistic action of fasting/starvation and sorafenib, we performed proteomics comparing p53WT and p53KO samples from cells and xenografts treated with sorafenib and starvation or sorafenib and fasted, respectively. Overall, 5064 proteins were reproducibly detected and quantified in all triplicate experiments with the p53WT and p53KO cells and the concomitant p53WT and p53KO xenografts. Of these, 2770 proteins were significantly changed, as determined by using analysis of variance (ANOVA) testing [false discovery rate (FDR), 0.05]. Hierarchical clustering correctly assigned replicates to experimental groups and identified four clearly distinct clusters of expression profiles (Fig. 6A). While clusters 1 and 4 are largely composed of proteins with varying expression levels in cells and xenografts, clusters 2 and 3 show proteins whose expression profiles were influenced in a similar way by p53KO (Fig. 6A). As the activity of p53 has been shown to be confined to transcriptional activation (*43*), we focused on cluster 3 containing 147 proteins down-regulated in p53KO samples (Fig. 6B). To further distinguish between direct and indirect effects of p53 KO, we overlapped these 147 proteins with high-confidence p53 targets derived from a previous meta-analysis (*44*). From this approach, only eight p53 targets emerged in our proteomic dataset as consistently down-regulated through p53KO both in vivo and in vitro (Fig. 6, C and D). Consistent with increased apoptosis upon combination treatment (Fig. 1, K and L), the proapoptotic regulator BAX was among the eight candidates (Fig. 6D), which was confirmed on protein and mRNA level for cells (Fig. 6, E and F) and xenografts (Fig. 6, G and H).

We next established that two other proapoptotic proteins, Bcl-2 homologous antagonist/killer (BAK1) and Bcl-2-binding component 3, isoforms 1/2 (BBC3 or PUMA), described to be regulated by p53 (*41*) but not detected in the proteomic analysis, were down-regulated in p53KO groups (Fig. 6, E to H). These data suggest that p53 is essential to prime HCC cells for apoptosis, resulting in higher susceptibility to intrinsic cell death upon combination treatment.

Periodic fasting improves sorafenib action in nonresistant cells and an orthotopic HCC mouse model

To investigate sorafenib/starvation synergism beyond the alleviation of resistance in late-stage HCC, we used sorafenib-responsive HCC-derived cell lines Huh6 clone 5, HuH-7, and JHH-5 (Fig. 7, A to C). Simultaneous starvation, however, significantly improved sorafenib efficacy in all three cell lines, implying a synergistic anticancer effect in nonresistant HCC cells.

To test whether this sorafenib-enhancing effect of starvation can be recapitulated in an orthotopic HCC mouse model, we treated mice with a single dose of diethylnitrosamine (DEN), a well-established protocol to induce HCC nodules in livers within months (*45*). The mice used were transgenic for a liver-specific conditional KO of *Trp53* [AlbCreER^{T2} X p53$^{lox/lox}$ mice (*46*); fig. S6, A to D]. In this model, p53KO was successfully established (Fig. 7D) through oral gavage of tamoxifen (100 mg/kg) after liver nodules developed (ultrasound imaging; fig. S6E) and before the treatment protocol was started (Fig. 7E). This experimental timeline was important to dissociate the impact of p53 status on treatment effects from long-term effects of p53 deficiency on tumorigenesis, as would be expected in a germline p53KO model (*47*). After 4 weeks of treatment (ad libitum fed + sorafenib or fasted + sorafenib), total body weight measured after refeeding phases (Fig. 7F) was unchanged. In addition to terminal liver weight (Fig. 7G), we found that, in p53-proficient HCC, nodule weight was reduced in the fasted/sorafenib group as compared to the fed/sorafenib group (Fig. 7H, top, and whole-liver photographs, bottom). However, in the p53KO group, this fasting-mediated reduction was absent, indicating that p53 is necessary for sorafenib-potentiating effects of periodic fasting (Fig. 7H), reminiscent of the situation in p53KO HepG2 xenografts (Fig. 4, G and H). Combination treatment also decreased nodule numbers in p53-proficient livers of DEN-treated mice (fig. S6F). In line with the changes in HCC nodule weight, concentrations of plasma markers of liver injury such as aspartate aminotransferase (AST), alanine transaminase (ALT), and lactate dehydrogenase (LDH) were notably lower in the p53WT group after combination treatment when compared to the p53KO group (Fig. 7I). This could not be ascribed to differential degrees of cirrhosis, which could not be detected in our model (fig. S6G). However, other liver markers remained unchanged (fig. S6H). Furthermore, the expression of glucose transporters 1 and 2 was decreased in p53KO HCC nodules in the combination treatment group in comparison to nodules in p53-proficient livers (Fig. 7J). This result is in line with the reduced glucose uptake shown in p53KO

Downloaded from https://www.science.org on February 16, 2022

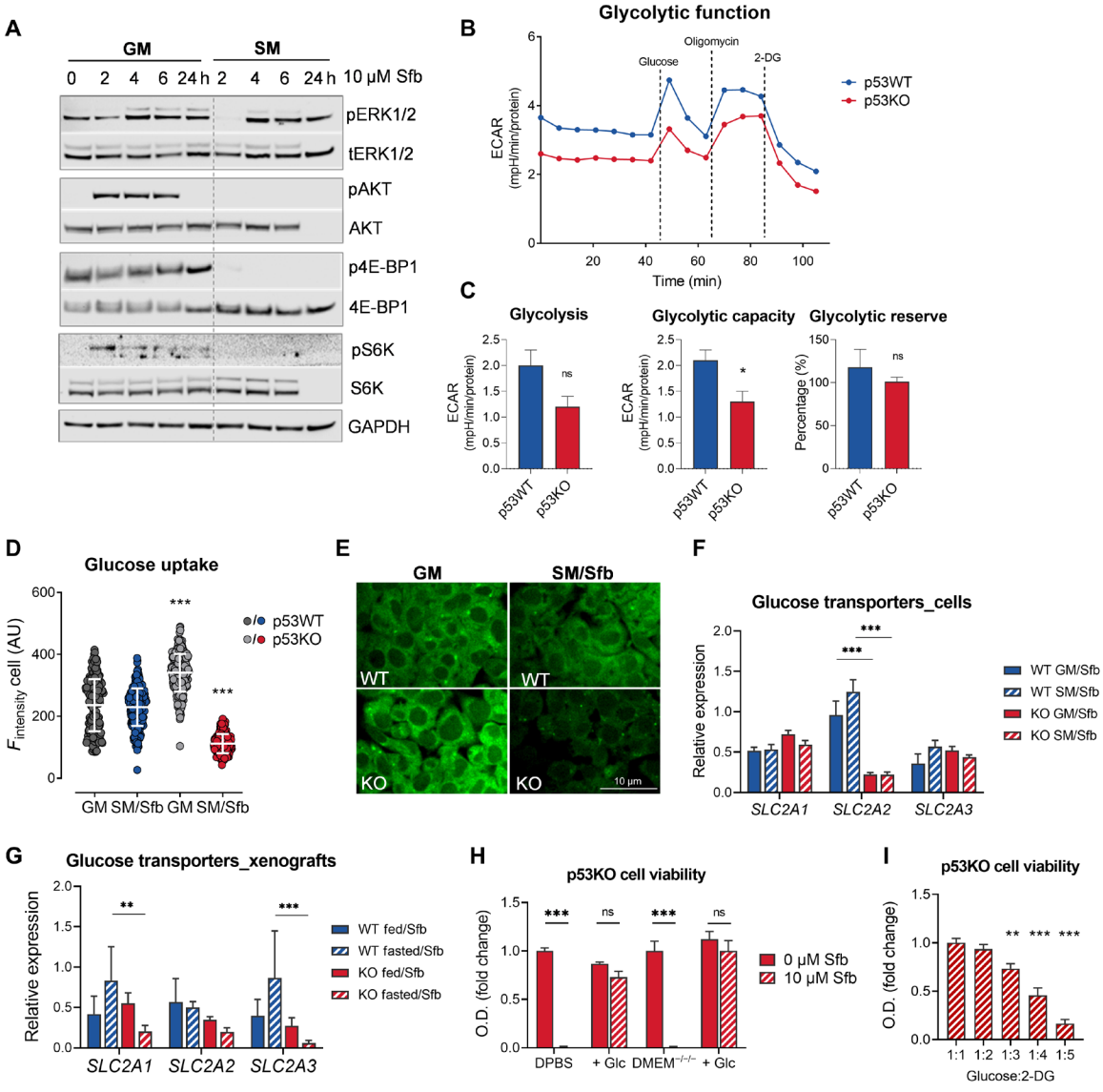

Fig. 5. p53 confers starvation/sorafenib synergism by regulating glycolytic rate and capacity. (**A**) p53KO HepG2 cells were grown in GM or SM with 10 μM sorafenib (Sfb) for the indicated times, and Western blot analysis was performed to determine protein levels of AKT, ERK, 4E-BP1, and S6K and their respective phosphorylated forms. GAPDH served as a loading control. (**B** and **C**) Glycolysis stress test in HepG2 p53WT and p53KO cells grown in GM for 24 hours. Unpaired *t* test was performed. (**D**) Glucose uptake measurement in p53WT and p53KO cells kept in GM or SM with 10 μM Sfb for 6 hours. One-way ANOVA and Tukey's multiple comparisons test were performed. Comparison of all groups versus GM is shown. (**E**) Representative images from the glucose uptake assay. (**F**) Expression of *SLC2A1*, *SLC2A2*, and *SLC2A3* determined in HepG2 WT and KO cells after a 24-hour incubation. Relative to reference genes *PPIA* and *B2m*. (**G**) Expression of *SLC2A1*, *SLC2A2*, and *SLC2A3* determined in HepG2 WT and KO xenografts after 4 weeks of treatment. Relative to reference genes *PPIA* and *B2m*. (**H**) Viability of p53KO HepG2 cells kept in DPBS or DMEM$^{-/-/-}$ alone or with the addition of 25 mM glucose with or without 10 μM Sfb for 24 hours. (**I**) Viability of p53KO HepG2 cells kept for 24 hours in GM supplemented with 10 μM Sfb and with the addition of 2-DG in indicated molar ratios to glucose. One-way ANOVA and Tukey's multiple comparisons test were performed. Comparison of all groups versus 1:1 group is shown. If not noted otherwise, mean values ± SEM are shown, and two-way ANOVA and Tukey's multiple comparisons test were performed. ***$P < 0.001$, **$P < 0.01$, and *$P < 0.05$; ns, not significant ($P > 0.05$).

HepG2 cells (Fig. 5, D and E) and the reduction of glucose transporter expression in p53KO cells and xenografts (Fig. 5, F and G). Moreover, a trend to reduced glucose and lactate levels and markedly increased β-hydroxybutyrate levels in HCC nodules in the fasted/sorafenib group (fig. S6I) indicated that fasting affects metabolite concentrations in the tumor microenvironment. The proapoptotic genes *Bak1*, *Bax*, and *Puma* were down-regulated in the p53KO groups and/or by combination treatment (Fig. 7K). Collectively, our data from nonresistant HCC cell lines and the orthotopic HCC mouse model indicate a therapy-enhancing effect of starvation/fasting in combination with sorafenib, warranting further studies to determine whether sorafenib can be used in earlier-stage, nonresistant HCC when combined with fasting regimens.

DISCUSSION

Our study provides evidence that nutrient restriction can alleviate sorafenib resistance in human HCC models and that it can improve

Downloaded from https://www.science.org on February 16, 2022

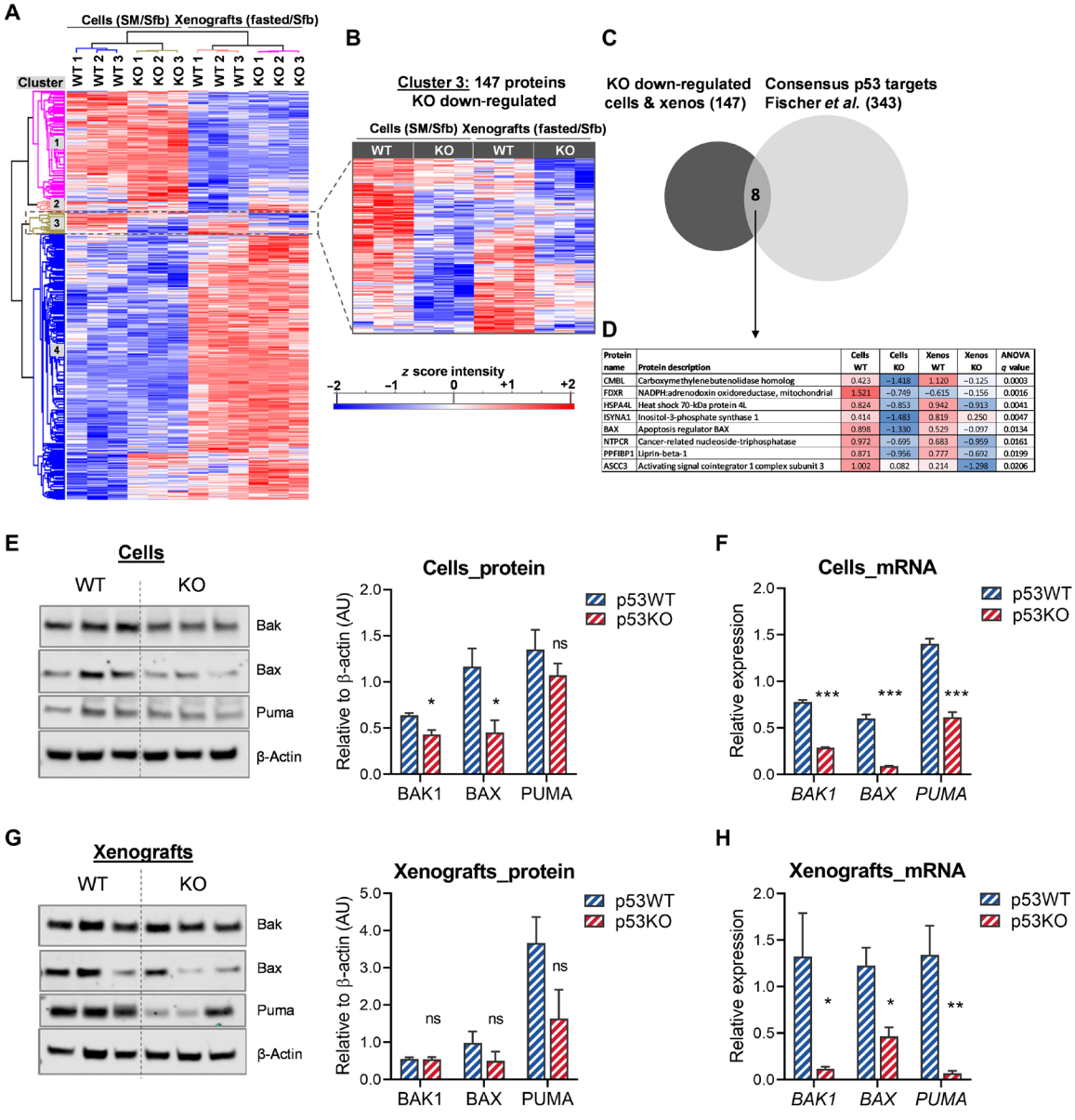

Fig. 6. p53 coordinates the proapoptotic proteome during combination treatment. (**A**) Heatmap of proteomic analysis from lysates derived from p53WT and p53KO HepG2 cells or xenografts. Xenografts from fasted and sorafenib-treated mice as described in Figs. 1A and 4D were used. HepG2 cells were grown in SM with 10 μM sorafenib (Sfb) for 6 hours. Proteins detected in all samples were submitted to ANOVA testing (FDR, 0.05) and to hierarchical clustering using Perseus. Values are displayed as *z* score. (**B**) Heatmap of 147 proteins from cluster 3. Values are displayed as *z* score. (**C**) Cluster 3 proteins were overlapped with biochemically verified p53 target genes (*44*). (**D**) Eight proteins from the overlap are shown with averaged *z* scores and ANOVA *q* values. (**E**) Western blot analysis and densitometric quantification measuring BAX, BAK, and PUMA protein levels from p53WT and p53KO cells after a 6-hour treatment with 10 μM Sfb in SM. Samples from three independent experiments were used. β-Actin served as a loading control. (**F**) qPCR expression analysis for samples as in (E). Relative to reference genes *PPIA* and *B2M*. (**G**) Western blot analysis and densitometric quantification measuring BAX, BAK, and PUMA protein levels from p53WT and p53KO xenografts after 4 weeks of fasted/Sfb combination treatment. Samples from three different xenografts with the same treatment were used. β-Actin served as a loading control. (**H**) qPCR expression analysis for samples as in (E). Relative to reference genes *PPIA* and *B2M*. If not noted otherwise, mean values ± SEM are shown, and unpaired *t* test was performed. ***$P < 0.001$, **$P < 0.01$, and *$P < 0.05$; ns, not significant ($P > 0.05$).

sorafenib efficacy in nonresistant settings. Our data establish a metabolic synergy between sorafenib-mediated OXPHOS inhibition and glucose limitation by nutrient restriction, imposing a "double whammy" on cancer cell metabolism (Fig. 8). This observation, if generalizable, creates a range of novel combination therapy opportunities for HCC treatment: the combination of glucose-limiting regimens or antiglycolytic agents with OXPHOS inhibitors. In support of this principle, previous studies have shown that suppression of glycolysis through targeting Hexokinase-II (*48*, *49*) or LDH (*50*) increased sorafenib efficacy, consistent with our results in nonresistant models (Fig. 7). In HuH-7 cells, combined treatment with sorafenib and the pyruvate dehydrogenase kinase inhibitor dichloroacetate

Downloaded from https://www.science.org on February 16, 2022

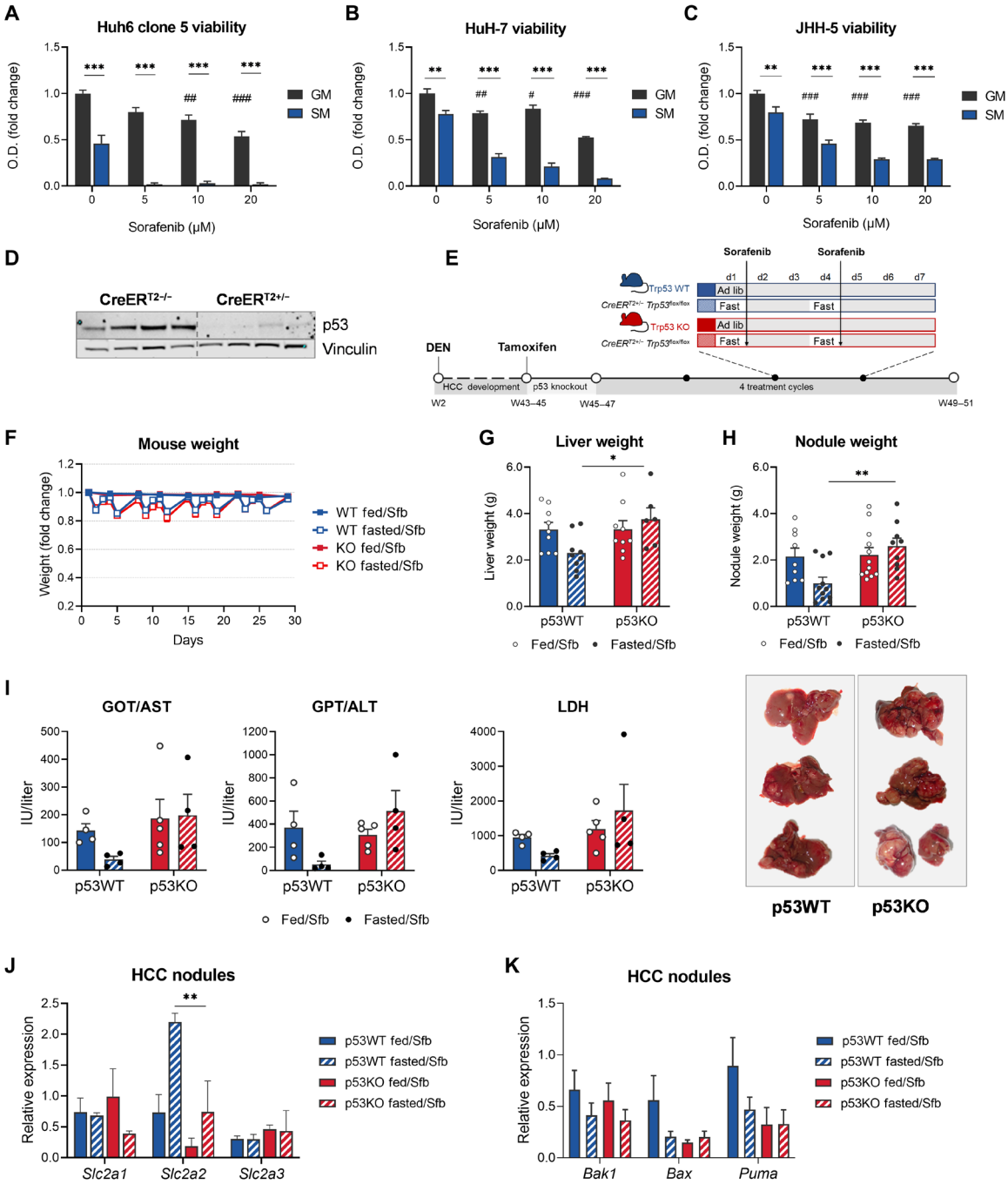

Fig. 7. Periodic fasting improves sorafenib action in nonresistant cells and an orthotopic HCC mouse model. (**A**) Huh6 clone 5, (**B**) HuH-7, and (**C**) JHH-5 cell lines were kept in GM or SM with 0, 5, 10, and 20 μM sorafenib (Sfb). Viability assay was performed after 24 hours of incubation. Comparison between GM and SM groups (*), and versus control and GM group (#), is shown. (**D**) Western blot to assess p53KO in the livers. Vinculin served as a loading control. (**E**) Experimental design (described in Materials and Methods). (**F**) Animal weight during the 4-week protocol. (**G**) Liver weight relative to body weight at the end of the experiment. (**H**) HCC whole-nodule weight relative to body weight at the end of the experiment (top). Photographs of livers from the fasted/Sfb groups at the end of the experiment (bottom). (**I**) Concentrations of ALT, AST, and LDH in the plasma on the sacrifice day in mice from designated groups. (**J**) Expression of glucose transporter genes determined in HCC nodules from fed/Sfb and fasted/Sfb groups. Relative to reference genes *Ppia* and *B2m*. (**K**) Expression of proapoptotic genes determined in HCC nodules from fed/Sfb and fasted/Sfb groups. Relative to reference genes *Ppia*β and *B2m*. If not noted otherwise, mean values ± SEM are shown, and two-way ANOVA and Tukey's multiple comparisons test were performed. *** and $^{###}P < 0.001$, ** and $^{##}P < 0.01$, and $^{*}P < 0.05$; ns, not significant ($P > 0.05$).

Downloaded from https://www.science.org on February 16, 2022

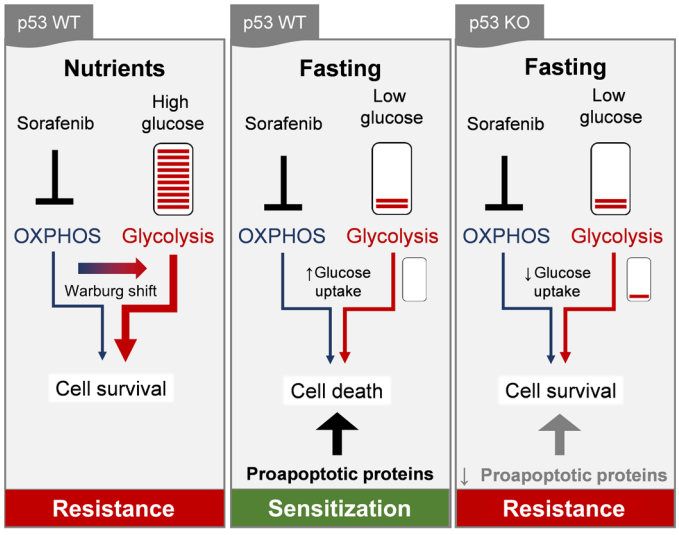

Fig. 8. Summary scheme of p53-dependent synergism between fasting and sorafenib. In resistant HCC models, sorafenib works noncanonically to inhibit OXPHOS, leading to a shift to glycolysis and survival under a nutrient-rich condition. Low glucose under fasting and starvation quenches glycolytic flux and sensitizes HCC cells to sorafenib action. Nonfunctional p53 prevents this sensitization through a reduction of the glucose uptake rate (leading to a more economic use of the available glucose under fasting) and through diminished expression of proapoptotic proteins, ultimately promoting survival under combination treatment. In addition, fasting/starvation improves sorafenib efficacy in nonresistant models.

(DCA) (*51*) or aspirin (which inhibits glycolysis via PFKPFB3 inhibition) reversed acquired sorafenib resistance. Such attempts have been shown to be successful in other cancer entities as well. For instance, the combination of glucose restriction and metformin (shown to act as a mitochondrial complex I inhibitor) (*52*) led to restriction of tumor growth in mice xenografted with colon cancer or melanoma cells (*53*). Although the primary mechanisms of action are clearly distinct for sorafenib and metformin, the fact that both can function as OXPHOS inhibitors, together with the excellent clinical safety profile of metformin, should instigate studies evaluating metformin/dietary restriction combinations for HCC therapy. Collectively, these examples, together with our results, indicate that targeting mitochondrial metabolism can be successfully combined with strategies that curb glycolysis (*54*). However, pharmacologic targeting of glycolysis might elicit adverse effects on nontransformed cells (*54*) or provoke the emergence of cancer cells that develop resistance by switching to utilization of other metabolites or nutrients (*55*). The pleiotropic and systemic effects of fasting on growth pathways and on the availability of various metabolites [including, but not limited to, glucose (*5*, *6*, *56*)], on the other hand, could squelch alternative tumorigenic pathways while being safe for nontransformed cells that have evolved coping with frequent fasting periods (*5*). The first clinical trials that evaluate fasting as an adjuvant to cancer therapy attest a positive safety profile (*5*, *57*). One limitation of these approaches could be that some patients with cancer are metabolically compromised (due to, e.g., liver steatosis, cachexia, and cirrhosis in HCC) and that sorafenib is only tested and recommended for well-compensated Child-Pugh A liver disease (*21*). However, our results show beneficial effects of combination therapy at relatively low sorafenib doses. For patients, a dose of ~10 mg/kg of body weight is given every day throughout treatment time. This would be equivalent to ~120 mg/kg daily in mice (*58*), while we only applied up to 60 mg/kg twice a week. In addition, we chose rather mild fasting regimens that allow for complete weight regain in the refeeding periods. As we see significant synergistic or additive effects already with these moderate conditions, it could be argued that moderate fasting/glucose reduction can be used to improve the efficacy of sorafenib at lower doses. This would reduce adverse effects and possibly make sorafenib amenable to patients with cirrhotic HCC beyond the Child-Pugh A population. In any case, careful evaluation of parameters such as cachexia, sarcopenia, and liver function markers will be important for stratification of patients for fasting as adjuvant therapy. Another potential translational limitation is the toxicity of combination therapy approaches. In this respect, our observation that sorafenib (30 mg/kg) with periodic fasting and sorafenib (60 mg/kg) with FMD led to a similar reduction in xenograft growth (Fig. 1) indicates that effective drug doses could be modified by the stringency and frequency of the concomitant dietary restriction. Another important translational consideration is the timing of application of the respective combination therapy regimens. Our choice to apply sorafenib after fasting or FMD is in line with findings of other studies that report improved drug efficacy only if applied after or during a ketogenic diet (*59*) or a fast (*53*). This emphasizes the importance of targeting cancer metabolism at a glucose/glycogen-depleted state and is likely to be relevant for the clinical implication of metabolic combination therapies.

In line with our data on p53, a more recent study in melanoma and breast cancer cells showed the Rev1-p53 axis as necessary for the antitumorigenic effects of starvation through regulating the expression of proapoptotic genes during combined treatment (*60*). Our data in HepG2 cells suggest a similar priming to intrinsic cell death (*61*) in cells proficient for p53, whereas p53 loss led to reduced expression of proapoptotic players. In particular, the proapoptotic effector Bax, shown to be a direct transcriptional target of p53 (*62*), was consistently down-regulated in vitro and in vivo, possibly allowing p53KO cells to resist apoptotic stimuli through the relatively short starvation periods in our starvation/fasting protocols. Since BH3 mimetics have been shown to sensitize HCC-derived cells to sorafenib (*63*), this might be a useful additional therapy to overcome the reinstated resistance in p53KO entities.

Besides alleviating resistance, fasting also improved drug efficacy in sorafenib-responsive cell lines that are WT (HepG2 and Huh6) and mutant (HuH-7 and JHH-5) for p53 (*64*). While JHH-5 cells harbor an in-frame deletion that does not compromise p53 and p21 protein abundance (*65*), it was reported that HuH-7 cells express mutated p53 protein that does not translocate into the nuclei. However, it was shown to still be sufficient to induce apoptosis through posttranscriptional mechanisms (*66*). Hence, it is conceivable that, in HuH-7 cells, mutated p53 confers its effects through apoptotic priming as suggested through our proteomic screen in HepG2 cells. Further studies are warranted to shed light on the specific action of HCC-relevant p53 mutants.

In addition to p53-mediated apoptosis, we found down-regulation of several glucose transporters in the HepG2 xenografts and HCC nodules of DEN-treated mice in p53-deficient versus p53-proficient samples. Although reporter assays showed a repressive effect of p53 on *GLUT1* (*SLC2A1*) and *GLUT4* (*SLC2A4*) promoters (*67*), p53 may be necessary for the regulation of glucose transporters in the chromatin context or in a cellular context that might involve a certain

Downloaded from https://www.science.org on February 16, 2022

set of p53 effectors, including microRNAs. However, the requirement of p53 for an effective Warburg shift in HCC cells is in agreement with p53's role as tumor suppressor, coordinating not only cell cycle progression and apoptosis but also, in particular, cancer cell metabolism (*41*, *42*).

Together, the data presented here could open new therapeutic windows to improve late-stage HCC therapy and should inspire clinical trials that apply fasting/sorafenib combination therapy, even for early/mid-stage HCC where currently no molecular therapy is efficacious. Furthermore, our data on p53 are clinically meaningful as these suggest to include a patient's p53 status in the diagnostic panel before embarking on such combination therapy.

MATERIALS AND METHODS

Cell culture

HepG2 and Huh6 clone 5 cell lines were purchased from the American Type Culture Collection and were cultivated in GM consisting of DMEM (Gibco, Life Technologies) containing 25 mM (4.5 g/liter) D-glucose, supplemented with 4 mM L-glutamine (GlutaMAX, Gibco, Life Technologies), 10% FCS (GE Healthcare Life Sciences), and penicillin-streptomycin (500 U/ml; Gibco, Life Technologies) at 37°C in humidified atmosphere with 5% CO_2. SM consisted of HBSS with $CaCl_2$ and $MgCl_2$ (Gibco, Life Technologies) containing 5.5 mM (1 g/liter) D-glucose, supplemented with 10 mM Hepes (Gibco, Life Technologies). HuH-7 and JHH-5 cell lines were purchased from JCRB. HuH-7 cells were grown in low-glucose (1 g/liter) DMEM with 10% FCS and penicillin-streptomycin (500 U/ml), while JHH-5 [established by S. Nagamori (*68*)] cells were grown in Williams' E medium with 10% FCS and penicillin-streptomycin (500 U/ml).

The following cell culture supplements were used: 2-DG (Santa Cruz Biotechnology), D-glucose (Sigma-Aldrich), sodium pyruvate (Gibco, Life Technologies), Dulbecco's phosphate-buffered saline (PBS; Gibco, Life Technologies), and DMEM without D-glucose, L-glutamine, and sodium pyruvate (Gibco, Life Technologies). The following therapeutics were used: sorafenib (LC Laboratories) and doxorubicin (Pfizer). Sorafenib was dissolved in dimethyl sulfoxide (DMSO) to 10 mM stock solution for cell culture use. The following inhibitors were used: SCH772984 ERK1/2 inhibitor (Cayman Chemicals); U0126 MEK inhibitor (Promega); wortmannin (HY-10197), buparlisib (HY-70063), and MK-2206 dihydrochloride (HY-10358), all from MedChemExpress; bafilomycin A1 (BioMol); and rapamycin (Life Technologies, NOVEX).

Primary mouse hepatocytes

C57BL/6J mice were anesthetized with ketamine (Pfizer)/xylazine (Bayer) (8 to 1.2%) mixture (4 μl/g). Liver was perfused by pumping (4 ml/min for 5 min) a prewarmed perfusion buffer (EBSS without $CaCl_2$/$MgCl_2$ with 0.5 mM EGTA; Gibco, Life Technologies) through a catheter inserted into the vena cava. Liver was then digested by a prewarmed digestion buffer consisting of HBSS and 5000 U of collagenase I (Worthington Biochemical). The liver was then excised and cut on ice in GM and passed through a cell strainer. The cell suspension was centrifuged at 770 rpm for 3 min to obtain a cell pellet. Afterward, the pellet was resuspended in 25 ml of GM and 25 ml of Percoll buffer (Biochrom) (containing 5 ml of 10× PBS and 45 ml of Percoll) and centrifuged at 770 rpm for 10 min. The supernatant containing dead cells was discarded, and the pellet was again resuspended in 25 ml of GM and centrifuged. Cells (2×10^5) were seeded on collagen I (Corning)–coated plates in GM.

Patient-derived organoid culture

Patient HCC-derived organoids (the sorafenib-resistant HCC-1 line) were provided by M.H. (Max Planck Institute, Dresden, Germany) (*28*). As described in the original publication (*28*), human specimens were obtained from liver tumor resections performed at the Erasmus Medical Center Rotterdam (MEC-2013-143), Cambridge University Hospitals NHS Trust (REC: 15/LO/0753, approval by NRES Committee London-Westminster), and the Royal Infirmary Hospital Edinburgh (REC: 15/ES/0097). Handling and processing of samples were performed according to HTA guidelines. The Cambridge samples were provided by the Cambridge Biorepository for Translational Medicine. All patients provided informed consent. Samples were procured, and the study was conducted under the Institutional Review Board of the Wellcome Trust/CRUK Gurdon Institute, University of Cambridge, UK approval before tissue acquisition (*28*).

Organoids were thawed and expanded as previously described (*29*). For experiments, organoids were harvested from two fully dense 50-μl Matrigel droplets (two wells from a 24-well plate) and seeded in 5-μl droplets per well in a 96-well plate, with 50 μl of media. GM was the same as the organoid expansion medium (*29*), and the organoid SM comprised three parts of organoid expansion medium [with glucose (3.1 g/liter)] and seven parts of DMEM without glucose. Final glucose concentration in organoid SM was 0.93 g/liter, similar to SM used with cell lines that contained glucose (1 g/liter). Organoids were kept in GM or SM with or without sorafenib and/or 2-DG for 6 days, with media and sorafenib replenishment every 2 days. Then, a viability assay was performed.

Viability assay

For the viability assay, 2×10^5 cells were seeded per well in a 96-well plate (Thermo Fisher Scientific) in 200 μl of GM to reach full confluency. Cells were allowed to attach for 24 hours at 37°C and 5% CO_2. After that, the medium was discarded, and cells were washed with PBS. Next, cells were treated as described in Results. Cell viability was analyzed using EZ4U assay (Biomedica Immunoassays) according to the manufacturer's instructions. Briefly, at the end of treatment, the medium was replaced with fresh GM (200 μl per well) and 20 μl per well of EZ4U working solution. After 2 hours of incubation at 37°C, the absorbance was measured at 492 nm with a reference wavelength of 620 nm (Spark 10M multimode microplate reader).

Gentian violet staining

The medium was discarded, and the cells were stained by adding Carbol gentian violet solution (Roth). After 15 min of incubation, cells were washed with deionized water several times until the dye stopped coming off. The cells were allowed to dry at room temperature.

Real-time apoptosis and necrosis assay

For the analysis of apoptosis and necrosis, the RealTime-Glo Annexin V Apoptosis and Necrosis Assay (Promega) was used. HepG2 cells (2×10^4) were seeded per well in a 96-well plate (F-bottom, white-bottomed, Greiner) in 200 μl of GM and cultivated for 24 hours at 37°C and 5% CO_2 for attachment. After 24 hours of incubation, GM was removed, and cells were washed with PBS. Cells were supplied with 100 μl of either phenol red–free GM or SM before addition of 100 μl of the detection reagents according to the manufacturer's

Downloaded from https://www.science.org on February 16, 2022

instructions. Luminescence and fluorescence were measured 0, 2, 4, 6, 8, 24, and 26 hours after treatment. Measurements were conducted at 37°C using orbital averaging as a scan mode with a scan diameter of 4 mm. Luminescence was measured at an emission wavelength of 470 to 480 nm with a gain of 3600- and 5-mm focal height. Fluorescence was measured at an excitation range of 485 ± 10 nm and collected in an emission range of 525 ± 20 with a gain of 1000 and a 5-mm focal height (CLARIOstar Plus, BMG Labtech).

Flow cytometry annexin V/7-AAD analysis

HepG2 cells (1×10^6) were seeded in 24-well plates (Thermo Fisher Scientific) and cultivated in GM for 24 hours in a humidified atmosphere with 5% CO_2 at 37°C. Subsequently, the medium was changed to either fresh GM or SM, and cells were treated with sorafenib for 24 or 48 hours. Cells were then labeled according to the manual of the fluorescein isothiocyanate annexin V apoptosis detection kit with 7-AAD (BioLegend), with a modification where the amount of 7-AAD was doubled.

LDH assay

Cells were seeded and treated as described for the viability assay. An LDH cytotoxicity assay kit (Takara) was used according to the manual provided, with a modification where the supernatant was diluted 10 times to stay in the measurable range of the photometer (SPARK 10M TECAN).

Western blot

Cultured cells were scraped and collected in radioimmunoprecipitation assay (RIPA) buffer including PhosStop and protease inhibitor cocktail (Roche). Xenograft and HCC mouse samples were homogenized in RIPA buffer using metal beads and the LT TissueLyser (Qiagen). All samples were sonicated (ultrasound probe, 3310 s at 10% output) and centrifuged. The clear supernatant was used to measure protein concentration with a bicinchoninic acid assay (Thermo Fisher Scientific). An amount of 30 μg of protein of each sample was used for Western blotting. The following antibodies were used: pERK1/2 (4370), ERK1/2 (4695), pAKT (4060), AKT (4691), p4E-BP1 (2855), 4E-BP1 (9452), phospho-p70 S6 kinase (9206), p70 S6 kinase (9202), glyceraldehyde-3-phosphate dehydrogenase (GAPDH; 2118S), p21 (2947S), Bak (12105), and Bax (5023), all from Cell Signaling Technologies; p53 (DO-1, sc-126, Santa Cruz Biotechnology), vinculin (PA5-29688, Invitrogen), LC3 (NB100-2220, NOVUS), ACTB (ab6276, Abcam), and Puma (sc-374223, Santa Cruz Biotechnology). The densitometric quantification of signal intensities was performed with Image Studio Lite (LI-COR Biosciences).

Generating a stable p53 KO cell line using the CRISPR-Cas9 system

CRISPR KO plasmids were provided by Santa Cruz Biotechnology (sc-416469), and the experiments were performed according to the manual. HepG2 cells (1×10^6) were seeded in a six-well plate in antibiotic-free GM 72 hours before transfection. At a confluence of 60%, cells were transfected with 1.5 μg of the control or KO plasmids by using 10 μl of UltraCruz transfection reagent (sc-395739). The selection of positive clones was performed by growing the cells in GM containing puromycin (sc-108071; 2 μg/ml) for 10 days. Cells were analyzed, and red fluorescent protein–positive (RFP^+) clones were isolated via fluorescence-activated cell sorting (FACS; FACSAria IIu, BD Biosciences). Then, single-cell cloning was performed to isolate RFP^+ populations derived from a single cell. Different clones were transfected again (the same protocol as the first transfection) with a plasmid expressing a CRE recombinase (sc-418923) and afterward analyzed again via FACS. RFP^- cells were isolated and analyzed via Western blot and qPCR to validate the complete KO of p53.

Overexpression of p53 by electroporation

Electroporation was performed using the Neon Transfection System 100-μl kit (Thermo Fisher Scientific) following the manufacturer's instructions. Cells (2×10^6; either HepG2 WT or HepG2 KO cells) were used for each electroporation. As vectors, 2 μg of pcDNA3 flag p53 or 2 μg of HisMax as a vehicle control was used. The pulse conditions voltage/width/pulses were set to 1400/30/1. The transfected cells were seeded in the appropriate cell number in 96-well plates and cultivated for 24 hours in GM under standard conditions.

RNA isolation and qPCR

RNA isolation was done using the PeqGOLD Total RNA Kit according to the manufacturer's instructions. RNA concentration was measured with NanoDrop (ND-1000, spectrophotometer, peqLab). Isolated RNA was reverse-transcribed to cDNA according to the Thermo Fisher Scientific RevertAid RT Kit using a random hexamer primer mix (1 μl). The samples (total volume of 12 μl), consisting of the template RNA (either 1 μg, 500 ng, or 200 ng) diluted in nuclease-free water and the primer(s), were incubated at 65°C for 5 min in the DNA Engine Dyad Peltier Thermal Cycler (Bio-Rad). Afterward, the following reagents were added: 5× reaction buffer (4 μl), RiboLock ribonuclease inhibitor (20 U/μl, 1 μl), 10 mM dNTP, this is a common term mix (2 μl), and RevertAid RT (200 U/μl, 1 μl). The samples were then incubated in the thermal cycler for 5 min at 25°C, followed by 60 min at 42°C, and 5 min at 70°C. The cDNA samples were diluted to 1 ng/μl and stored at −20°C. qPCR was done in 96- or 384-well plates. Therefore, either 2.5 μl of cDNA (1 ng/μl), 5 μl of SYBR Green (Bio-Rad), and 2.5 μl of primer mix (800 nM, forward and reverse) per reaction in a 96-well plate or 1.5 μl of cDNA, 3 μl of SYBR Green, and 2 μl of primer mix per reaction in a 384-well plate were used. Primer sequences are given in table S1. qPCR was performed with the CFX96 or CFX384 Real-Time System (C1000 Thermal Cycler, Bio-Rad) according to the program as follows: 1 cycle (10 min) at 95°C; 40 cycles: 15 s at 95°C, 1 min at 60°C, and 1 min at 72°C; 1 cycle: 30 s at 95°C, 30 s at 60°C, and 30 s at 95°C.

Mitochondrial stress test and glycolysis stress test

To obtain confluent monolayers, 2×10^5 cells per well were plated in five technical replicates on collagen-coated XF96 polystyrene cell culture microplates (Seahorse, Agilent) in GM and left to adhere overnight. Cells were then incubated in GM or SM with DMSO or sorafenib as indicated in Results, and these reagents were added in all subsequent media during the measurement. For OCR measurements, cells that were kept in GM were washed and incubated in XF base medium (Agilent) containing 1 mM sodium pyruvate, 2 mM glutamine, and 25 mM D-glucose, and cells that were kept in SM were washed and incubated in HBSS (without Hepes) containing 5.5 mM glucose. For ECAR measurements, cells were incubated in glucose-free DMEM (D5030, Millipore Sigma) supplemented with 2 mM glutamine. An XF96 extracellular flux analyzer (Seahorse, Agilent, CA, USA) was used. After calibration of the analyzer, sequential compound injections, including oligomycin A (4 μM), carbonyl cyanide *p*-trifluoromethoxyphenylhydrazone (FCCP; 0.2 μM), and

Downloaded from https://www.science.org on February 16, 2022

antimycin A (2.5 μM), were applied to test mitochondrial respiration. Sequential compound injections, including glucose (10 mM), oligomycin A (1 μM), and 2-DG (50 mM), were applied to test glycolytic activity. OCR (in picomol of O_2 per minute) and ECAR (in mpH per minute) values were normalized to protein content.

Mitochondrial membrane potential measurements

Cells (5×10^5) were seeded in GM per collagen-coated round glass in a six-well plate and left overnight to attach. The next day, medium was changed to GM with vehicle (DMSO) or sorafenib, and cells were incubated for 2 or 6 hours. Untreated cells in GM served as a control. The mitochondrial membrane potential was assessed using tetramethylrhodamine (TMRM; T668, Invitrogen) staining according to the manufacturer's protocol. Cells were incubated with 20 nM TMRM at 37°C for 20 min in the dark and then washed with PBS. The $\Delta\psi_{mito}$ value was obtained by application of 1 μM FCCP. Imaging was performed on an inverted fluorescence microscope based on an IX73 Olympus stage (IX73 system) with a 40× objective and a Retiga R1 charge-coupled device (CCD) camera (Teledyne QImaging). Cells were excited at 550 nm, and emission was captured at 600 nm.

MitoTracker green staining

Cells (1×10^6) were seeded in GM per collagen-coated round glass in a six-well plate and left overnight to attach. The next day, medium was changed to GM with vehicle (DMSO) or sorafenib, and cells were incubated for 2 or 6 hours. Untreated cells were used as a control. Cells were incubated with MitoTracker green (0.5 μM) (M7514, Invitrogen) in GM for 3 hours at 37°C. The mitochondrial structure was observed under an array confocal laser scanning microscope (ACLSM), based on a Zeiss Observer Z.1 inverted microscope, equipped with a YokogawaCSU-X1 Nipkow spinning disk system, a piezoelectric *z*-axis motorized stage (CRWG3-200; NipponThompson Co. Ltd., Tokyo, Japan), and a CoolSNAP HQ2 CCD Camera (Photometrics Tucson), using a 100× objective. The cells were excited at a wavelength of 488 nm, and emission was captured at 516 nm.

Glucose uptake measurements

Cells (1.5×10^6) were seeded in GM per collagen-coated round glass in a six-well plate and left overnight to attach. The next day, medium as changed to GM or SM with vehicle (DMSO) or sorafenib, and cells were incubated for 2 or 6 hours. Untreated cells were used as a control. For glucose uptake analysis, 2-NBDG glucose uptake marker (Thermo Fisher Scientific) was used. Cells were glucose-depleted for 10 min before measurement in loading buffer containing 2 mM $CaCl_2$, 135 mM NaCl, 5 mM KCl, 1 mM $MgCl_2$, 1 mM Hepes, 2.6 mM $NaHCO_3$, 0.44 mM KH_2PO_4, 0.34 mM sodium phosphate buffer, 0.1% vitamins, 0.2% essential amino acids, and 1% penicillin/streptomycin (Gibco), all at pH. After 10 min, 2-NBDG was applied to the cells for the staining in a 0.1 mM concentration, and the cells were incubated at 37°C for 30 min. Afterward, the cells were washed three times with a loading buffer and imaged in the same buffer. The imaging experiments were performed at an ACLSM, based on a Zeiss Observer Z.1 inverted microscope, equipped with a YokogawaCSU-X1 Nipkow spinning disk system, a piezoelectric *z*-axis motorized stage (CRWG3-200; NipponThompson Co. Ltd.), and a CoolSNAP HQ2 CCD Camera (Photometrics Tucson), using a 40× objective. The glucose uptake marker 2-NBDG was excited with a wavelength of 488 nm, and the emission was captured at 516 nm. Data acquisition and control were done using the VisiView Premier Acquisition software (2.0.8, Visitron Systems). For imaging analysis, MetaMorph (Molecular Devices) was used. For the calculation of the average intensity of the cytosolic fluorescence signal, first, the ACLSM images were background-subtracted on MetaMorph using a background region of interest. MetaMorph software was applied by setting a region around the cell and performing an average intensity calculation.

Immunohistochemistry

Immunohistochemical staining of formalin-fixed, paraffin-embedded xenografts was performed after antigen retrieval (120°C, 7 min at pH 9) and peroxidase blocking (Dako) using the UltraVision LP detection system (Thermo Fisher Scientific) according to the manual with Ki-67 antibody (1 ng/ml; M728; Dako). For color reaction, AEC (3-amino-9-ethyl carbazole) chromogen (Thermo Fisher Scientific) was used. Counterstaining with hematoxylin was done on all slides. Quantitative analysis was performed by Halo image analysis platform (Indica Labs) using random forest tissue classifier. Picrosirius red staining was used to assess cirrhosis in HCC nodules of DEN-treated mice.

Proteomics

Mouse-derived xenograft HCC tumors were homogenized in RIPA buffer using metal beads and the LT TissueLyser (Qiagen). Samples were sonicated (Branson Sonifier 3310 s ultrasound probe, 10% output), centrifuged at 14,000 rpm for 5 min, and quantified with bicinchoninic acid (BCA) assay (Thermo Fisher Scientific). Cell culture (HepG2 WT and HepG2 KO) samples were scraped from the cell culture wells in RIPA buffer and directly sonicated, centrifuged, and quantified. A total of 250 μg of each sample was precipitated with a methanol/chloroform protocol (*69*). The protein pellet was reconstituted in 100 mM tris (pH 8.5) and 2% sodium deoxycholate (SDC) and reduced/alkylated with 5 mM TCEP/30 mM chloroacetamide at 56°C for 10 min. The proteins were subjected to proteolysis with 1:100 Lys-C and 1:50 trypsin overnight at 37°C. Digestion was stopped by adding 1% trifluoroacetic acid to a final concentration of 0.5%. Precipitated SDC was removed by centrifugation at 14,000 rpm for 10 min, and the supernatant containing digested peptides was desalted on an Oasis HLB plate (Waters). Peptides were dried and dissolved in 2% formic acid before liquid chromatography–tandem mass spectrometry (MS/MS) analysis. A total of 3000 ng of the mixture of tryptic peptides was analyzed using an Ultimate3000 high-performance liquid chromatography system (Thermo Fisher Scientific) coupled online to a Q Exactive HF-x mass spectrometer (Thermo Fisher Scientific). Buffer A consisted of water acidified with 0.1% formic acid, while buffer B was 80% acetonitrile and 20% water with 0.1% formic acid. The peptides were first trapped for 1 min at 30 μl/min with 100% buffer A on a trap (0.3 mm by 5 mm with PepMap C18, 5 μm, 100 Å; Thermo Fisher Scientific); after trapping, the peptides were separated by a 50-cm analytical column packed with C18 beads (Poroshell 120 EC-C18, 2.7 μm; Agilent Technologies). The gradient was 9 to 40% B in 155 min at 400 nl/min. Buffer B was then raised to 55% in 10 min and increased to 99% for the cleaning step. Peptides were ionized using a spray voltage of 1.9 kV and a capillary heated at 275°C. The mass spectrometer was set to acquire full-scan MS spectra (350 to 1400 mass/charge ratio) for a maximum injection time of 120 ms at a mass resolution of 120,000 and an automated gain control (AGC) target value of 3×10^6. Up to 25 of the most intense precursor ions were selected

Downloaded from https://www.science.org on February 16, 2022

for MS/MS. HCD fragmentation was performed in the HCD cell, with the readout in the Orbitrap mass analyzer at a resolution of 15,000 (isolation window of 1.4 Th) and an AGC target value of 1×10^5 with a maximum injection time of 25 ms and a normalized collision energy of 27%.

Proteomic data analysis

All raw files were analyzed by MaxQuant v1.6.17 software using the integrated Andromeda search engine and searched against the Human UniProt Reference Proteome (October 2020 release with 75,088 protein sequences) alone for cells, while for xenograft, we added the Mouse UniProt Reference Proteome (October 2020 release with 55,489 protein sequences) (*70*). MaxQuant was used with the standard parameters (the "label-free quantification" and "match between runs" were selected with automatic values) with only the addition of deamidation (N) as variable modification. Data analysis was then carried out with Perseus v1.6.14: Proteins reported in the file "proteinGroups.txt" were filtered for reverse, potential contaminants and identified by site. For the quantitation, we used the label-free quantification calculated by MaxQuant, and we kept only proteins found in at least two biological replicates in each group; in xenografts, we eliminated proteins that were only identified in the Mouse Fasta. At this point, missing values were imputed by Perseus with the automatic settings (width, 0.3; down shift, 1.8; mode, separately for each column), leading to 5064 proteins left for statistical analysis with ANOVA testing (Benjamini-Hochberg FDR, 0.05), *z* score (mean per row), and hierarchical clustering. The MS proteomic data have been deposited to the ProteomeXchange Consortium via the PRIDE (*71*) partner repository with the dataset identifier PXD022723.

In vivo experiments

All experiments were performed in accordance with the European Directive 2010/63/EU and approved by the Austrian Federal Ministry of Education, Science and Research. Mice were housed under standard 12-hour light/12-hour dark cycles. Sorafenib was first dissolved in DMSO (120 mg/ml) and then diluted in polyethylene glycol (PEG) 400:PBS (1:1) in a final working concentration of 3 mg/ml. Mice received sorafenib (30 mg/kg) by oral gavage.

Xenograft assays

HepG2 WT or KO cells (2×10^6) in 100 μl of PBS:Matrigel (1:1) were injected into both hind flanks of 6-week-old male NMRI-*Foxn1*^{nu} mice. In one experiment, once the tumors were measurable (>100 mm^3, 14 to 21 days after injection), the mice were randomly assigned to four groups (n = 6 to 10 per group), receiving either vehicle control [DMSO in PEG 400:PBS (1:1)] or sorafenib via oral gavage in groups that were kept on ad libitum diet (Altromin 1320 fortified) or on a periodic fasting regimen, meaning that the mice were withheld food for 24 hours two times a week (with ad libitum access to water and hydrogel), with 2 or 3 days of ad libitum refeeding in between. Sorafenib or vehicle control was applied at the beginning of the refeeding phase and at a concentration of 30 mg/kg. In the second experiment, once the tumors were measurable, the mice were randomly assigned to four groups (n = 6 to 10 per group), receiving either vehicle control [DMSO in PEG 400:PBS (1:1)] or sorafenib via oral gavage in groups that were kept on ad libitum diet (Altromin 1320 fortified) or fed FMD, with ad libitum access to water and hydrogel. Mice were kept on ad libitum diet for 5 days between the FMD cycles. The protocol was repeated for 4 cycles. Sorafenib or vehicle control was applied at the beginning and at the end of FMD feeding at a concentration of 60 mg/kg. FMD was purchased from Prolon and was prepared as already published (*25*) to accommodate 50% of the average calorie intake on day 1 and 10% of average calorie intake on day 2. Average food intake was calculated for all mice based on their standard chow intake 1 week in advance.

Xenografts were measured with a caliper once a week, and tumor volume was calculated using a formula as follows: $V = (4/3) \times \pi \times (L/2) \times (L/2) \times (W/2)$, with L as length (shorter dimension) and W as width (longer dimension). At the end of the fourth fasting cycle, mice were refed for 3 to 4 days and then sacrificed. Some mice were sacrificed after an additional 24-hour fast.

Double transgenic mice

Tp53$^{flox/flox}$ C57BL/6J mice were crossed with CreER$^{T2+/-}$ C57BL/6J mice to generate Tp53$^{flox/flox}$ CreER$^{T2+/-}$ mice and the respective Tp53$^{flox/flox}$ CreER$^{T2-/-}$ controls (*46*).

Pilot experiments

Pilot experiments were performed to establish the most effective periodic fasting protocol and safe sorafenib concentrations. In the first pilot experiment, C57BL/6J mice (n = 6 per group) were fasted for 24 hours with 48 hours of refeeding in between, while in the second pilot experiment, C57BL/6J mice (n = 7 per group) were fasted every other day for 1 week. Food intake and body weight were measured daily. For NMR measurements, blood was collected from the submandibular vein immediately before animals were sacrificed, after the last fasting day. Between 100 and 300 μl of blood was mixed with 10 μl of EDTA and kept at room temperature for a maximum of 30 min. Then, samples were centrifuged at 4°C at 3500 rpm for 10 min. Plasma was transferred to clean tubes and stored at −80°C until measurement.

A third pilot experiment was performed to assess the liver toxicity of sorafenib. C57BL/6J mice (n = 6 per group) received vehicle or 10, 30, or 50 mg/kg of sorafenib by oral gavage three times per week for four consecutive weeks. Mice were weighed two times per week (when gavaged). At the end of the experiment, mice were sacrificed, and liver pieces were formalin-fixed and paraffin-embedded for further analyses.

Isolation of interstitial fluid and blood glucose measurement

Xenografts were dissected within 2 min after the mice were sacrificed by cervical dislocation. They were weighed, briefly washed in PBS, put on a cell sieve with 20-μm pores (pluriStrainer, 20 μm, Pluriselect) on top of a 50-ml tube, and centrifuged at 300*g* at 4°C for 10 min. Flow-through interstitial fluid was collected (5 to 100 μl per xenograft). Glucose concentration in the interstitial fluid was measured by the Glucose colorimetric/Fluorometric Assay Kit (Merck), according to the manufacturer's instructions. Five microliters of interstitial fluid was used per measurement. Blood glucose was measured by tail vein puncture using an Accu-Check Guide glucometer (Roche).

NMR metabolite analysis

To extract polar metabolites, 140 μl of ice-cold methanol was added to 70 μl of plasma, the tube mixed by shaking, and stored at −20°C for 1 hour. Tubes were centrifuged at 13,000 rpm for 30 min (4°C), the supernatant was transferred to a fresh tube, and the samples were lyophilized. For NMR experiments, samples were redissolved in 500 μl of NMR buffer {0.08 M sodium phosphate buffer, 5 mM

Downloaded from https://www.science.org on February 16, 2022

TSP [3-(trimethylsilyl) propionic acid-2,2,3,3-d4 sodium salt], 0.04% (w/v) NaN_3 in D2O, pH adjusted to 7.4 with 8 M HCl and 5 M NaOH}. Plasma metabolic analysis was conducted at 310 K using a Bruker Advance Neo 600 MHz NMR spectrometer equipped with a TXI probe head. The Carr-Purcell-Meiboom-Gill pulse sequence was used to acquire ^{1}H one-dimensional NMR spectra with presaturation for water suppression (cpmgpr1d, 512 scans, 73,728 points in F1, 12019.230 Hz spectral width, 1024 transients, recycle delay of 4 s). NMR spectral data were processed as previously described (*72*). Shortly, data were processed in Bruker Topspin version 4.0.2 using one-dimensional exponential window multiplication of the FID, Fourier transformation, and phase correction. NMR data were then imported to Matlab2014b, TSP was used as an internal standard for chemical shift referencing (set to 0 parts per million), regions around the water, TSP and methanol signals were excluded, NMR spectra were aligned, and a probabilistic quotient normalization was performed. Quantification of metabolites was carried out by signal integration of normalized spectra.

Orthotopic HCC model in double transgenic mice

DEN (N0756, Sigma-Aldrich) was diluted in 0.9% sterile NaCl to a working concentration of 2.5 mg/ml. Male $CreER^{T2+/-}$ and $CreER^{T2-/-}$ $Tp53^{flox/flox}$ C57BL/6J mice received DEN (25 mg/kg, i.p.) at the age of 2 weeks. After 41 to 43 weeks, after developing HCC, the mice received tamoxifen (100 mg/kg) by oral gavage for five consecutive days, followed by a 1-week washout phase. Tamoxifen (Molekula) was prepared fresh as a working solution (30 mg/ml) in 90% peanut oil and 10% ethanol. Then, 4 cycles of treatment were conducted: Mice were either fed ad libitum or fasted two times per week for 24 hours in the periodically fasted group. Both groups received sorafenib (30 mg/kg) by oral gavage two times per week, after the 24-hour fasting in the fasted group, and on the same day in the fed group. After 4 cycles and an additional 2 to 3 days of ad libitum feeding, the mice were sacrificed. The whole liver was weighed, then all HCC nodules were dissected from the liver and weighed together to assess total tumor mass.

Ultrasound

Briefly, mice were anesthetized using isoflurane (2 liters/min of O_2, 4% isoflurane in the anesthesia chamber; 2 liters/min of O_2, 2% isoflurane in the anesthesia mask during imaging). Anesthetized animals were shaved and fixed lying down on the working bench. Ultrasound imaging was performed using Vevo 3100 (FUJIFILM VisualSonics).

Liver biochemistry

Liver panel strips (Menarini SPOTCHEM II, Liver-1 33925) were used for the quantitative determination of LDH, AST, ALT, albumin, total protein, and total bilirubin in mouse plasma (by Spotchem EZ SP-4430 Arkray Inc.). Briefly, blood was collected from the submandibular vein immediately before animals were sacrificed. Between 100 and 300 µl of blood was mixed with 10 µl of EDTA and left at room temperature for a maximum of 30 min. Then, samples were centrifuged at 4°C at 3500 rpm for 10 min. Plasma was transferred to clean tubes and stored at −80°C until measurement. For the panel measurements, 70 µl of plasma was loaded.

Statistical analysis

If not stated otherwise, all experiments were performed at least three times independently. Statistical analyses were performed using GraphPad Prism 8 (GraphPad Software). Statistically significant differences were determined as described in the figure legends. If not noted otherwise, data represent mean values ± SEM with the following grades of statistical significance: $*P < 0.05$, $**P < 0.01$, and $***P < 0.001$. Statistical proteomic analyses (ANOVA, *z* score, and hierarchical clustering) were performed using Perseus v1.6.14.0 (*73*).

SUPPLEMENTARY MATERIALS

Supplementary material for this article is available at https://science.org/doi/10.1126/sciadv.abh2635

View/request a protocol for this paper from *Bio-protocol*.

REFERENCES AND NOTES

1. T. G. Bivona, R. C. Doebele, A framework for understanding and targeting residual disease in oncogene-driven solid cancers. *Nat. Med.* **22**, 472–478 (2016).
2. D. Hanahan, R. A. Weinberg, Hallmarks of cancer: The next generation. *Cell* **144**, 646–674 (2011).
3. M. G. V. Heiden, L. C. Cantley, C. B. Thompson, Understanding the Warburg effect: The metabolic requirements of cell proliferation. *Science* **324**, 1029–1033 (2009).
4. J. Krstic, T. R. Pieber, A. Prokesch, in *International Review of Cell and Molecular Biology* (Elsevier Inc., ed. 1, 2020), vol. 354, pp. 231–259.
5. A. Nencioni, I. Caffa, S. Cortellino, V. D. Longo, Fasting and cancer: Molecular mechanisms and clinical application. *Nat. Rev. Cancer* **18**, 707–719 (2018).
6. V. D. Longo, M. P. Mattson, Fasting: Molecular mechanisms and clinical applications. *Cell Metab.* **19**, 181–192 (2014).
7. R. J. DeBerardinis, N. S. Chandel, Fundamentals of cancer metabolism. *Sci. Adv.* **2**, e1600200 (2016).
8. O. Warburg, On the origin of cancer cells. *Science* **123**, 309–314 (1956).
9. N. N. Pavlova, C. B. Thompson, The emerging hallmarks of cancer metabolism. *Cell Metab.* **23**, 27–47 (2016).
10. R. Buono, V. D. Longo, Starvation, stress resistance, and cancer. *Trends Endocrinol. Metab.* **29**, 271–280 (2018).
11. C. Vernieri, S. Casola, M. Foiani, F. Pietrantonio, F. de Braud, V. Longo, Targeting cancer metabolism: Dietary and pharmacologic interventions. *Cancer Discov.* **6**, 1315–1333 (2016).
12. M. Di Tano, F. Raucci, C. Vernieri, I. Caffa, R. Buono, M. Fanti, S. Brandhorst, G. Curigliano, A. Nencioni, F. de Braud, V. D. Longo, Synergistic effect of fasting-mimicking diet and vitamin C against KRAS mutated cancers. *Nat. Commun.* **11**, 2332 (2020).
13. S. Lévesque, J. G. Pol, G. Ferrere, L. Galluzzi, L. Zitvogel, G. Kroemer, Trial watch: Dietary interventions for cancer therapy. *Onco. Targets. Ther.* **8**, 1591878 (2019).
14. J. M. Llovet, R. K. Kelley, A. Villanueva, A. G. Singal, E. Pikarsky, S. Roayaie, R. Lencioni, K. Koike, J. Zucman-Rossi, R. S. Finn, Hepatocellular carcinoma. *Nat. Rev. Dis. Prim.* **7**, 6 (2021).
15. R. Sharma, Descriptive epidemiology of incidence and mortality of primary liver cancer in 185 countries: Evidence from GLOBOCAN 2018. *Jpn. J. Clin. Oncol.* **50**, 1370–1379 (2020).
16. P. A. Farazi, R. A. DePinho, Hepatocellular carcinoma pathogenesis: From genes to environment. *Nat. Rev. Cancer* **6**, 674–687 (2006).
17. J. M. Llovet, R. Montal, D. Sia, R. S. Finn, Molecular therapies and precision medicine for hepatocellular carcinoma. *Nat. Rev. Clin. Oncol.* **15**, 599–616 (2018).
18. R. S. Finn, S. Qin, M. Ikeda, P. R. Galle, M. Ducreux, T.-Y. Kim, M. Kudo, V. Breder, P. Merle, A. O. Kaseb, D. Li, W. Verret, D.-Z. Xu, S. Hernandez, J. Liu, C. Huang, S. Mulla, Y. Wang, H. Y. Lim, A. X. Zhu, A.-L. Cheng, Atezolizumab plus bevacizumab in unresectable hepatocellular carcinoma. *N. Engl. J. Med.* **382**, 1894–1905 (2020).
19. Y. Hou, B. Wu, Atezolizumab plus bevacizumab versus sorafenib as first-line treatment for unresectable hepatocellular carcinoma: A cost-effectiveness analysis. *Cancer Commun.* **40**, 743–745 (2020).
20. Y. J. Zhu, B. Zheng, H. Y. Wang, L. Chen, New knowledge of the mechanisms of sorafenib resistance in liver cancer. *Acta Pharmacol. Sin.* **38**, 614–622 (2017).
21. J. M. Llovet, S. Ricci, V. Mazzaferro, P. Hilgard, E. Gane, J. F. Blanc, A. C. De Oliveira, A. Santoro, J. L. Raoul, A. Forner, M. Schwartz, C. Porta, S. Zeuzem, L. Bolondi, T. F. Greten, P. R. Galle, J. F. Seitz, I. Borbath, D. Häussinger, T. Giannaris, M. Shan, M. Moscovici, D. Voliotis, J. Bruix, Sorafenib in advanced hepatocellular carcinoma. *N. Engl. J. Med.* **359**, 378–390 (2008).
22. O. Lo Re, C. Panebianco, S. Porto, C. Cervi, F. Rappa, S. Di Biase, M. Caraglia, V. Pazienza, M. Vinciguerra, Fasting inhibits hepatic stellate cells activation and potentiates anti-cancer activity of sorafenib in hepatocellular cancer cells. *J. Cell. Physiol.* **233**, 1202–1212 (2018).
23. C. Fucile, S. Marenco, M. Bazzica, M. L. Zuccoli, F. Lantieri, L. Robbiano, V. Marini, P. Di Gion, G. Pieri, P. Stura, A. Martelli, V. Savarino, F. Mattioli, A. Picciotto, Measurement

Downloaded from https://www.science.org on February 16, 2022

of sorafenib plasma concentration by high-performance liquid chromatography in patients with advanced hepatocellular carcinoma: Is it useful the application in clinical practice? A pilot study. *Med. Oncol.* **32**, 335 (2015).
24. H. Mai, J. Huang, Y. Zhang, N. Qu, H. Qu, G. H. Mei, J. Liu, X. Xu, L. Chen, In-vivo relation between plasma concentration of sorafenib and its safety in Chinese patients with metastatic renal cell carcinoma: A single-center clinical study. *Oncotarget* **8**, 43458–43469 (2017).
25. S. Brandhorst, I. Y. Choi, M. Wei, C. W. Cheng, S. Sedrakyan, G. Navarrete, L. Dubeau, L. P. Yap, R. Park, M. Vinciguerra, S. Di Biase, H. Mirzaei, M. G. Mirisola, P. Childress, L. Ji, S. Groshen, F. Penna, P. Odetti, L. Perin, P. S. Conti, Y. Ikeno, B. K. Kennedy, P. Cohen, T. E. Morgan, T. B. Dorff, V. D. Longo, A periodic diet that mimics fasting promotes multi-system regeneration, enhanced cognitive performance, and healthspan. *Cell Metab.* **22**, 86–99 (2015).
26. J. M. Lee, M. Wagner, R. Xiao, K. H. Kim, D. Feng, M. A. Lazar, D. D. Moore, Nutrient-sensing nuclear receptors coordinate autophagy. *Nature* **516**, 112–115 (2014).
27. A. Prokesch, F. A. Graef, T. Madl, J. Kahlhofer, S. Heidenreich, A. Schumann, E. Moyschewitz, P. Pristoynik, A. Blaschitz, M. Knauer, M. Muenzner, J. G. Bogner-Strauss, G. Dohr, T. J. Schulz, M. Schupp, Liver p53 is stabilized upon starvation and required for amino acid catabolism and gluconeogenesis. *FASEB J.* **31**, 732–742 (2017).
28. L. Broutier, G. Mastrogiovanni, M. M. A. Verstegen, H. E. Francies, L. M. Gavarró, C. R. Bradshaw, G. E. Allen, R. Arnes-Benito, O. Sidorova, M. P. Gaspersz, N. Georgakopoulos, B. K. Koo, S. Dietmann, S. E. Davies, R. K. Praseedom, R. Lieshout, J. N. M. IJzermans, S. J. Wigmore, K. Saeb-Parsy, M. J. Garnett, L. J. W. Van Der Laan, M. Huch, Human primary liver cancer-derived organoid cultures for disease modeling and drug screening. *Nat. Med.* **23**, 1424–1435 (2017).
29. L. Broutier, A. Andersson-Rolf, C. J. Hindley, S. F. Boj, H. Clevers, B.-K. Koo, M. Huch, Culture and establishment of self-renewing human and mouse adult liver and pancreas 3D organoids and their genetic manipulation. *Nat. Protoc.* **11**, 1724–1743 (2016).
30. C. Jian, J. Fu, X. Cheng, L. J. Shen, Y. X. Ji, X. Wang, S. Pan, H. Tian, S. Tian, R. Liao, K. Song, H. P. Wang, X. Zhang, Y. Wang, Z. Huang, Z. G. She, X. J. Zhang, L. Zhu, H. Li, Low-dose sorafenib acts as a mitochondrial uncoupler and ameliorates nonalcoholic steatohepatitis. *Cell Metab.* **31**, 892–908.e11 (2020).
31. I. El Dika, M. Capanu, J. F. Chou, J. J. Harding, M. Ly, A. D. Hrabovsky, R. K. G. Do, J. Shia, B. Millang, J. Ma, E. M. O'Reilly, G. K. Abou-Alfa, Phase II trial of sorafenib and doxorubicin in patients with advanced hepatocellular carcinoma after disease progression on sorafenib. *Cancer Med.* **9**, 7453–7459 (2020).
32. P. Merle, J. F. Blanc, J. M. Phelip, G. Pelletier, J. P. Bronowicki, Y. Touchefeu, G. Pageaux, R. Gerolami, F. Habersetzer, E. Nguyen-Khac, A. Casadei-Gardini, I. Borbath, A. Tran, H. Wege, A. S. Saad, M. Colombo, A. Abergel, C. Richou, I. Waked, N. S. Yee, A. Molé, P. Attali, J. Le Boulicaut, B. Vasseur, D. Moussata, J. D. Grangé, V. Ratziu, F. Khemissa-Akouz, H. Regnault, B. Dauvois, J. P. Zarski, I. Ollivier-Hourmand, S. Manfredi, M. Debette-Gratien, A. Gangloff, T. Fontanges, A. Baron, M. Bouattour, J. Vincent, W. Sieghart, A. Maieron, M. Peeters, J. Delwaide, L. Lasser, T. Berg, M. Schultheiß, A. Zipprich, J. Trojan, U. Ehmer, G. Luppi, G. Luca, S. Tamberi, D. Amoroso, O. Alabiso, A. Buonadonna, P. Toniutto, E. Tamburini, A. Cubillo, A. Muñoz, C. Guillén, G. Sánchez, H. Manzano, V. Navarro, I. Ales, B. Massuti, M. Dank, G. Bodoky, Z. Kahan, Z. Horváth, N. Gabrail, H. Ozer, C. Galanopoulos, R. Hauke, M. Raj, H. Harputluoglu, A. Sevinc, E. Goker, A. Coker, S. Yalcin, M. Ali, O. Ata, I. Tugba, M. ElKassas, A. Abdel, I. Wakid, S. Shamaa, N. El, H. Kohail, J. Makarem, I. Chehade, F. Farhat, C. López, M. Marín, Doxorubicin-loaded nanoparticles for patients with advanced hepatocellular carcinoma after sorafenib treatment failure (RELIVE): A phase 3 randomised controlled trial. *Lancet Gastroenterol. Hepatol.* **4**, 454–465 (2019).
33. S. M. Wilhelm, C. Carter, L. Y. Tang, D. Wilkie, A. McNabola, H. Rong, C. Chen, X. Zhang, P. Vincent, M. McHugh, Y. Cao, J. Shujath, S. Gawlak, D. Eveleigh, B. Rowley, L. Liu, L. Adnane, M. Lynch, D. Auclair, I. Taylor, R. Gedrich, A. Voznesensky, B. Riedl, L. E. Post, G. Bollag, P. A. Trail, BAY 43-9006 exhibits broad spectrum oral antitumor activity and targets the RAF/MEK/ERK pathway and receptor tyrosine kinases involved in tumor progression and angiogenesis. *Cancer Res.* **64**, 7099–7109 (2004).
34. P. I. Poulikakos, C. Zhang, G. Bollag, K. M. Shokat, N. Rosen, RAF inhibitors transactivate RAF dimers and ERK signalling in cells with wild-type BRAF. *Nature* **464**, 427–430 (2010).
35. P. Lito, N. Rosen, D. B. Solit, Tumor adaptation and resistance to RAF inhibitors. *Nat. Med.* **19**, 1401–1409 (2013).
36. G. Y. Liu, D. M. Sabatini, mTOR at the nexus of nutrition, growth, ageing and disease. *Nat. Rev. Mol. Cell Biol.* **21**, 183–203 (2020).
37. G. Hoxhaj, B. D. Manning, The PI3K–AKT network at the interface of oncogenic signalling and cancer metabolism. *Nat. Rev. Cancer* **20**, 74–88 (2020).
38. L. Fiume, M. Manerba, M. Vettraino, G. Di Stefano, Effect of sorafenib on the energy metabolism of hepatocellular carcinoma cells. *Eur. J. Pharmacol.* **670**, 39–43 (2011).
39. F. Paech, C. Mingard, D. Grünig, V. F. Abegg, J. Bouitbir, S. Krähenbühl, Mechanisms of mitochondrial toxicity of the kinase inhibitors ponatinib, regorafenib and sorafenib in human hepatic HepG2 cells. *Toxicology* **395**, 34–44 (2018).
40. R. L. Elstrom, D. E. Bauer, M. Buzzai, R. Karnauskas, M. H. Harris, D. R. Plas, H. Zhuang, R. M. Cinalli, A. Alavi, C. M. Rudin, C. B. Thompson, Akt stimulates aerobic glycolysis in cancer cells. *Cancer Res.* **64**, 3892–3899 (2004).
41. E. R. Kastenhuber, S. W. Lowe, Putting p53 in context. *Cell* **170**, 1062–1078 (2017).
42. C. F. Labuschagne, F. Zani, K. H. Vousden, Control of metabolism by p53—Cancer and beyond. *Biochim. Biophys. Acta Rev. Cancer* **1870**, 32–42 (2018).
43. M. Fischer, L. Steiner, K. Engeland, The transcription factor p53: Not a repressor, solely an activator. *Cell Cycle* **13**, 3037–3058 (2014).
44. M. Fischer, Census and evaluation of p53 target genes. *Oncogene* **36**, 3943–3956 (2017).
45. R. Tolba, T. Kraus, C. Liedtke, M. Schwarz, R. Weiskirchen, Diethylnitrosamine (DEN)-induced carcinogenic liver injury in mice. *Lab. Anim.* **49**, 59–69 (2015).
46. M. Schuler, F. Ali, E. Metzger, P. Chambon, D. Metzger, Temporally controlled targeted somatic mutagenesis in skeletal muscles of the mouse. *Genesis* **41**, 165–170 (2005).
47. L. A. Donehower, M. Harvey, B. L. Slagle, M. J. McArthur, C. A. Montgomery, J. S. Butel, A. Bradley, Mice deficient for p53 are developmentally normal but susceptible to spontaneous tumours. *Nature* **356**, 215–221 (1992).
48. D. DeWaal, V. Nogueira, A. R. Terry, K. C. Patra, S. M. Jeon, G. Guzman, J. Au, C. P. Long, M. R. Antoniewicz, N. Hay, Hexokinase-2 depletion inhibits glycolysis and induces oxidative phosphorylation in hepatocellular carcinoma and sensitizes to metformin. *Nat. Commun.* **9**, 446 (2018).
49. J.-J. Yoo, S. Yu, J. Na, K. Kim, Y. Cho, Y. Lee, E. Cho, J.-H. Lee, Y. Kim, H. Youn, J.-H. Yoon, Hexokinase-II inhibition synergistically augments the anti-tumor efficacy of sorafenib in hepatocellular carcinoma. *Int. J. Mol. Sci.* **20**, 1292 (2019).
50. L. Fiume, M. Vettraino, M. Manerba, G. Di Stefano, Inhibition of lactic dehydrogenase as a way to increase the anti-proliferative effect of multi-targeted kinase inhibitors. *Pharmacol. Res.* **63**, 328–334 (2011).
51. Y. C. Shen, D. L. Ou, C. Hsu, K. L. Lin, C. Y. Chang, C. Y. Lin, S. H. Liu, A. L. Cheng, Activating oxidative phosphorylation by a pyruvate dehydrogenase kinase inhibitor overcomes sorafenib resistance of hepatocellular carcinoma. *Br. J. Cancer* **108**, 72–81 (2013).
52. W. W. Wheaton, S. E. Weinberg, R. B. Hamanaka, S. Soberanes, L. B. Sullivan, E. Anso, A. Glasauer, E. Dufour, G. M. Mutlu, G. R. Scott Budigner, N. S. Chandel, Metformin inhibits mitochondrial complex I of cancer cells to reduce tumorigenesis. *eLife* **2014**, e02242 (2014).
53. M. Elgendy, M. Cirò, A. Hosseini, W. Weckwerth, M. Foiani, S. M. Correspondence, J. Weiszmann, L. Mazzarella, E. Ferrari, R. Cazzoli, G. Curigliano, A. Decensi, B. Bonanni, A. Budillon, P. G. Pelicci, V. Janssens, M. Ogris, M. Baccarini, L. Lanfrancone, S. Minucci, Combination of hypoglycemia and metformin impairs tumor metabolic plasticity and growth by modulating the PP2A-GSK3b-MCL-1 axis. *Cancer Cell* **35**, 798–815.e5 (2019).
54. K. Vasan, M. Werner, N. S. Chandel, Mitochondrial metabolism as a target for cancer therapy. *Cell Metab.* **32**, 341–352 (2020).
55. G. Grasmann, A. Mondal, K. Leithner, Flexibility and adaptation of cancer cells in a heterogenous metabolic microenvironment. *Int. J. Mol. Sci.* **22**, 1476 (2021).
56. M. Schupp, F. Chen, E. R. Briggs, S. Rao, H. J. Pelzmann, A. R. Pessentheiner, J. G. Bogner-Strauss, M. A. Lazar, D. Baldwin, A. Prokesch, Metabolite and transcriptome analysis during fasting suggest a role for the p53-Ddit4 axis in major metabolic tissues. *BMC Genomics* **14**, 758 (2013).
57. D. D. Weber, S. Aminzadeh-Gohari, J. Tulipan, L. Catalano, R. G. Feichtinger, B. Kofler, Ketogenic diet in the treatment of cancer—Where do we stand? *Mol. Metab.* **33**, 102–121 (2020).
58. A. Nair, S. Jacob, A simple practice guide for dose conversion between animals and human. *J. Basic Clin. Pharm.* **7**, 27–31 (2016).
59. B. D. Hopkins, C. Pauli, D. Xing, D. G. Wang, X. Li, D. Wu, S. C. Amadiume, M. D. Goncalves, C. Hodakoski, M. R. Lundquist, R. Bareja, Y. Ma, E. M. Harris, A. Sboner, H. Beltran, M. A. Rubin, S. Mukherjee, L. C. Cantley, Suppression of insulin feedback enhances the efficacy of PI3K inhibitors. *Nature* **560**, 499–503 (2018).
60. H. S. Shim, M. Wei, S. Brandhorst, V. D. Longo, Starvation promotes REV1 SUMOylation and p53-dependent sensitization of melanoma and breast cancer cells. *Cancer Res.* **75**, 1056–1067 (2015).
61. J. Lopez, S. W. G. Tait, Mitochondrial apoptosis: Killing cancer using the enemy within. *Br. J. Cancer* **112**, 957–962 (2015).
62. E. C. Thornborrow, S. Patel, A. E. Mastropietro, E. M. Schwartzfarb, J. J. Manfredi, A conserved intronic response element mediates direct p53-dependent transcriptional activation of both the human and murine bax genes. *Oncogene* **21**, 990–999 (2002).
63. A. Tutusaus, M. Stefanovic, L. Boix, B. Cucarull, A. Zamora, L. Blasco, P. G. de Frutos, M. Reig, J. C. Fernandez-Checa, M. Marí, A. Colell, J. Bruix, A. Morales, Antiapoptotic BCL-2 proteins determine sorafenib/regorafenib resistance and BH3-mimetic efficacy in hepatocellular carcinoma. *Oncotarget* **9**, 16701–16717 (2018).
64. S. Caruso, A. L. Calatayud, J. Pilet, T. La Bella, S. Rekik, S. Imbeaud, E. Letouzé, L. Meunier, Q. Bayard, N. Rohr-Udilova, C. Péneau, B. Grasl-Kraupp, L. de Koning, B. Ouine, P. Bioulac-Sage, G. Couchy, J. Calderaro, J. C. Nault, J. Zucman-Rossi, S. Rebouissou, Analysis of liver cancer cell lines identifies agents with likely efficacy against

Downloaded from https://www.science.org on February 16, 2022

hepatocellular carcinoma and markers of response. *Gastroenterology* **157**, 760–776 (2019).
65. M. Miyazaki, M. Sakaguchi, I. Akiyama, Y. Sakaguchi, S. Nagamori, N. H. Huh, Involvement of interferon regulatory factor 1 and S100C/A11 in growth inhibition by transforming growth factor β1 in human hepatocellular carcinoma cells. *Cancer Res.* **64**, 4155–4161 (2004).
66. X. Shi, J. Liu, L. Ren, N. Mao, F. Tan, N. Ding, J. Yang, M. Li, Nutlin-3 downregulates p53 phosphorylation on serine392 and induces apoptosis in hepatocellular carcinoma cells. *BMB Rep.* **47**, 221–226 (2014).
67. F. Schwartzenberg-Bar-Yoseph, M. Armoni, E. Karnieli, The tumor suppressor p53 down-regulates glucose transporters GLUT1 and GLUT4 gene expression. *Cancer Res.* **64**, 2627–2633 (2004).
68. K. Fujise, S. Nagamori, S. Hasumura, S. Homma, H. Sujino, T. Matsuura, K. Shimizu, M. Niiya, H. Kameda, K. Fujita, T. Ohno, Integration of hepatitis B virus DNA into cells of six established human hepatocellular carcinoma cell lines. *Hepato-Gastroenterology* **37**, 457–460 (1990).
69. D. Wessel, U. I. Flügge, A method for the quantitative recovery of protein in dilute solution in the presence of detergents and lipids. *Anal. Biochem.* **138**, 141–143 (1984).
70. J. Cox, M. Mann, MaxQuant enables high peptide identification rates, individualized p.p.b.-range mass accuracies and proteome-wide protein quantification. *Nat. Biotechnol.* **26**, 1367–1372 (2008).
71. Y. Perez-Riverol, A. Csordas, J. Bai, M. Bernal-Llinares, S. Hewapathirana, D. J. Kundu, A. Inuganti, J. Griss, G. Mayer, M. Eisenacher, E. Pérez, J. Uszkoreit, J. Pfeuffer, T. Sachsenberg, Ş. Yilmaz, S. Tiwary, J. Cox, E. Audain, M. Walzer, A. F. Jarnuczak, T. Ternent, A. Brazma, J. A. Vizcaíno, The PRIDE database and related tools and resources in 2019: Improving support for quantification data. *Nucleic Acids Res.* **47**, D442–D450 (2019).
72. S. Stryeck, M. Gastrager, V. Degoricija, M. Trbušić, I. Potočnjak, B. Radulović, G. Pregartner, A. Berghold, T. Madl, S. Frank, Serum concentrations of citrate, tyrosine, 2- and 3-hydroxybutyrate are associated with increased 3-month mortality in acute heart failure patients. *Sci. Rep.* **9**, 6743 (2019).
73. S. Tyanova, J. Cox, in *Methods in Molecular Biology* (Humana Press Inc., 2018), vol. 1711, pp. 133–148.

Acknowledgments: We thank S. Blass, H. Bischof, S. Wallner, R. Arnes-Benito, I. Vidakovic, and R. Prassl for technical and methodological help. We thank S. Brandhorst for advising on FMD preparation. We are grateful to M. Lazar, M. Schupp, R. Flores, A. Pessentheiner, E. Heitzer, and S. Frank for critical evaluation of the manuscript. We also thank P. Chambon, R. Moriggl, and D. Kaltenecker for making Alb-CreERT2 mice available and T. Schulz for providing p53-floxed mice. We are grateful to B. Huppertz for providing support at the Division of Cell Biology, Histology, and Embryology. **Funding:** J.K. was funded and supported by the Austrian Science Fund (FWF, grant P29328), by a grant of the Oesterreichische Nationalbank (Austrian Central Bank, Anniversary Fund, project number 18517), and by a MEFOgraz research grant. I.R. was funded by the PhD faculty MolMed at the Medical University of Graz. I.R., M.G., K.S., N.B., N.K., H.M., and C.N. were supported by the Austrian Science Fund (FWF, grants P29328 and I3165). A.P. was supported by the Austrian Science Fund (FWF, grants P29328, P34109, and I3165) and by a MEFOgraz grant from the Medical University of Graz. This work has also been supported by EPIC-XS (0000260), funded by the Horizon 2020 program of the European Union. T.M. was supported by the Austrian Science Foundation grants P28854, I3792, and DK-MCD W1226; Austrian Research Promotion Agency (FFG) grants 864690 and 870454; the Integrative Metabolism Research Center Graz; and Austrian Infrastructure Program 2016/2017, the Styrian Government (Zukunftsfonds), and BioTechMed-Graz (Flagship project). S.S., M.G., N.B., and N.K. were trained within the frame of the PhD program Molecular Medicine, Medical University of Graz. **Author contributions:** J.K. designed and performed the experiments, analyzed the data, and wrote the manuscript. I.R., K.S., N.B., N.K., E.M., M.A., H.M., Z.R., S.U., and C.N. performed experiments and analyzed data. M.R.D., J.R.-M., and S.S. performed and analyzed experiments on cell metabolism. M.G. and R.Z.C. performed and analyzed proteomic experiments. M.P., B.R., A.J.A.D., A.R., T.M., A.J.R.H., M.H., and R.M. contributed materials and provided expertise and feedback. A.P. designed, coordinated, and supervised the project; analyzed the data; and wrote the manuscript. **Competing interests:** M.H. is an inventor on a patent related to this work filed by KNAW (PCT/IB2011/002167) and published in February 2012. The authors declare that they have no other competing interests. **Data and materials availability:** All data needed to evaluate the conclusions in the paper are present in the paper and/or the Supplementary Materials. The MS proteomic data have been deposited to the ProteomeXchange Consortium via the PRIDE partner repository with the dataset identifier PXD022723. The HCC organoids can be provided by M.H. pending scientific review and a completed material transfer agreement.

Submitted 25 February 2021
Accepted 29 November 2021
Published 21 January 2022
10.1126/sciadv.abh2635

Downloaded from https://www.science.org on February 16, 2022

ScienceAdvances

Fasting improves therapeutic response in hepatocellular carcinoma through p53-dependent metabolic synergism

Jelena KrsticIsabel ReinischKatharina SchindlmaierMarkus GalhuberZina RiahiNatascha BergerNadja KupperElisabeth MoyschewitzMartina AuerHelene MichenthalerChristoph NössingMaria R. DepaoliJeta Ramadani-MujaSinem UsluerSarah StryeckMartin PichlerBeate RinnerAlexander J. A. DeutschAndreas ReinischTobias MadlRiccardo Zenezini ChiozziAlbert J. R. HeckMeritxell HuchRoland MalliAndreas Prokesch

Sci. Adv., 8 (3), eabh2635. • DOI: 10.1126/sciadv.abh2635

View the article online
https://www.science.org/doi/10.1126/sciadv.abh2635
Permissions
https://www.science.org/help/reprints-and-permissions

Downloaded from https://www.science.org on February 16, 2022

Use of think article is subject to the Terms of service

Science Advances (ISSN) is published by the American Association for the Advancement of Science. 1200 New York Avenue NW, Washington, DC 20005. The title *Science Advances* is a registered trademark of AAAS.
Copyright © 2022 The Authors, some rights reserved; exclusive licensee American Association for the Advancement of Science. No claim to original U.S. Government Works. Distributed under a Creative Commons Attribution NonCommercial License 4.0 (CC BY-NC).